PHOTOGRAPHIC OBSERVATIONS OF 10 ARTIFICIAL METEORS

W. G. AYERS, R. E. McCROSKY, C.-Y. SHAO

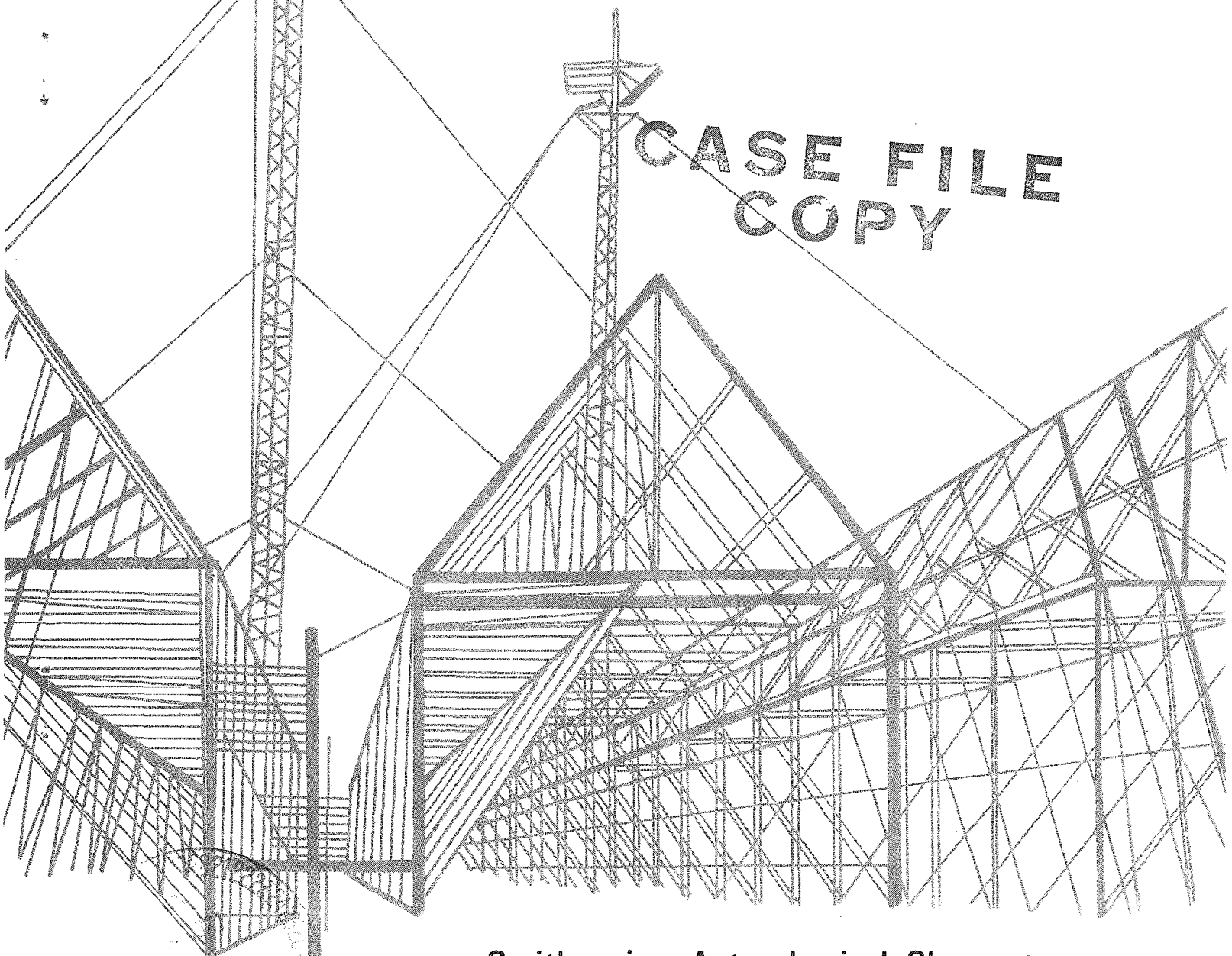

Smithsonian Astrophysical Observatory
SPECIAL REPORT 317

Research in Space Science
SAO Special Report No. 317

PHOTOGRAPHIC OBSERVATIONS OF 10 ARTIFICIAL METEORS

W. G. Ayers, R. E. McCrosky, and C.-Y. Shao

June 5, 1970

Smithsonian Institution
Astrophysical Observatory
Cambridge, Massachusetts 02138

912-136

TABLE OF CONTENTS

LIST OF FIGURES

LIST OF TABLES

ABSTRACT

A series of meteor-simulation experiments by rocket flights conducted during 1962 to 1967 produced seven iron and three nickel artificial meteors. The results from the photographic observations are presented. We have calculated the values of the luminous-efficiency factor for these meteors and have derived a relationship between the photographic luminous efficiency factor τ_{pg} and the velocity for the meteoritic iron and stone.

RÉSUMÉ

Des séries d'expériences pour simuler des météores par vols de fusées, faites entre 1962 et 1967, ont produit sept météores artificiels en fer et trois en nickel. Nous donnons les résultats obtenus à partir d'observations photographiques. Nous avons calculé pour ces météores les valeurs du facteur d'efficacité lumineuse et en avons dérivé une relation entre le facteur d'efficacité lumineuse photographique τ_{pg} et la vitesse pour le fer et la pierre météoritiques.

КОНСПЕКТ

Во время ракетных полетов, проводимых с 1962 по 1967 г., была проделана серия экспериментов по искуственному созданию метеоров: было получено 7 железных и 3 никелевых метеоров. Приводятся результаты фотографических наблюдений. Мы подсчитали величину светового кпд для этих метеоров и вывели отношение между фотографическим световым кпд (τ_{pg}) и скоростью метеоритного железа и камня.

PHOTOGRAPHIC OBSERVATIONS OF 10 ARTIFICIAL METEORS

W. G. Ayers, R. E. McCrosky, and C. -Y. Shao

1. INTRODUCTION

The luminosity of meteors depends, in part, on the meteoroid mass. Statistical studies of meteors suggest a form of the approximate law relating luminous energy to kinetic energy in the meteoric process (see, e. g., Verniani, 1967). In general, the observations cannot supply information on the proportionality constant, the luminous efficiency. In early studies of meteors, the value for the luminous efficiency coefficient τ was derived either from theoretical work or from observations of natural meteors. The various values of τ (e. g., Öpik, 1933, 1955; Whipple and Hawkins, 1959; Cook, 1955) differed by as much as two orders of magnitude, and thus one of the basic parameters in meteor physics was virtually unknown. The value of τ was first determined experimentally from the observations of an artificial iron meteor of known mass and composition (McCrosky and Soberman, 1963; hereafter referred to as MS). This experiment and other more recent studies of this problem, based on the analysis of certain special natural meteors (Cook, Jacchia, and McCrosky, 1963) and on laboratory experiments (Friichtenicht, Slattery, and Tagliaferri, 1968; hereafter FST), have placed useful limits on the luminosity coefficient.

The Langley Research Center (LRC), National Aeronautics and Space Administration (NASA), and the Smithsonian Astrophysical Observatory (SAO) have conducted a series of rocket-borne artificial-meteor experiments to confirm the earlier findings and to extend them to different materials and

This research was supported in part by Contract NSR 09-015-033 from the National Aeronautics and Space Administration.

velocities. This paper presents the results of the measurements of the photographic luminous efficiency of the artificial meteors.

SAO's participation in the optical observing program included the operation of a Super-Schmidt camera network. These cameras had been used by the Harvard College Observatory meteor program in the Southwest (Whipple, 1949) to produce the most extensive and useful photographic observations of natural meteors to date. A calibration of meteor phenomena as recorded by these specific instruments was considered a primary goal of the artificial-meteor program. Thus, the same x-ray (blue-sensitive) film used previously was also used for most of the artificial meteors.

NASA's participation in the optical observing program included the operation of a camera network composed of modified aerial and ballistic cameras. Panchromatic film was used primarily in these cameras to extend the photographic measurements to longer wavelengths.

Iron and nickel were chosen as the test materials in these experiments. Emission from both these materials is present in many meteor spectra. Neutral iron emission is by far the most prominent feature in the blue portion of spectra obtained from slow natural meteors. Although nickel is a relatively unimportant contributor to luminosity, it is fairly easy to launch from a shaped-charge device as an integral body. Other more interesting elements (e. g. , silicon, magnesium, and calcium) present launch problems well beyond the state of the art. Thus, criteria based on importance and simplicity determined the nature of the experiments.

2. EXPERIMENTS

From 1962 to 1967, seven rocket flights were successfully launched from NASA's Wallops Island Station, Virginia, producing 10 artificial meteors. Two rocket vehicle systems, the Nike-Cajun and the Trailblazer 2, were used for this program. The former was employed in four launches, the latter in three.

Both are multistage solid-fuel rocket systems developed by NASA. The Nike-Cajun (Figure 1) has six stages and produces two artificial meteors. It consists of two rocket motors (Nike and Cajun) as booster stages and a velocity package that contains two separate reentry systems. Each reentry system consists of a spherical rocket motor (Cygnus 5) and a shaped-charge accelerator containing the artificial-meteoroid material.

A trajectory for a typical Nike-Cajun flight is shown in Figure 2. The booster motors lift the velocity package to an apogee distance of about 110 km — an altitude above the height of natural meteors. The reentry systems are ignited sequentially soon after apogee, propelling the artificial meteoroids into the earth's atmosphere.

The Trailblazer 2 (Figure 3) vehicle has six stages and produces one artificial meteor. It has two booster stages (Castor and Thiokol TX-77) and a velocity package that contains a single reentry system. This reentry system consists of three rocket motors (Altair X-248, Cygnus 15, and Cygnus 5) and a shaped-charge accelerator containing the artificial-meteoroid material. By using several stages in the velocity package, the Trailblazer 2 vehicle is capable of producing reentry velocities several kilometers per second greater than is possible with the Nike-Cajun. A trajectory for a typical Trailblazer 2 flight is shown in Figure 4.

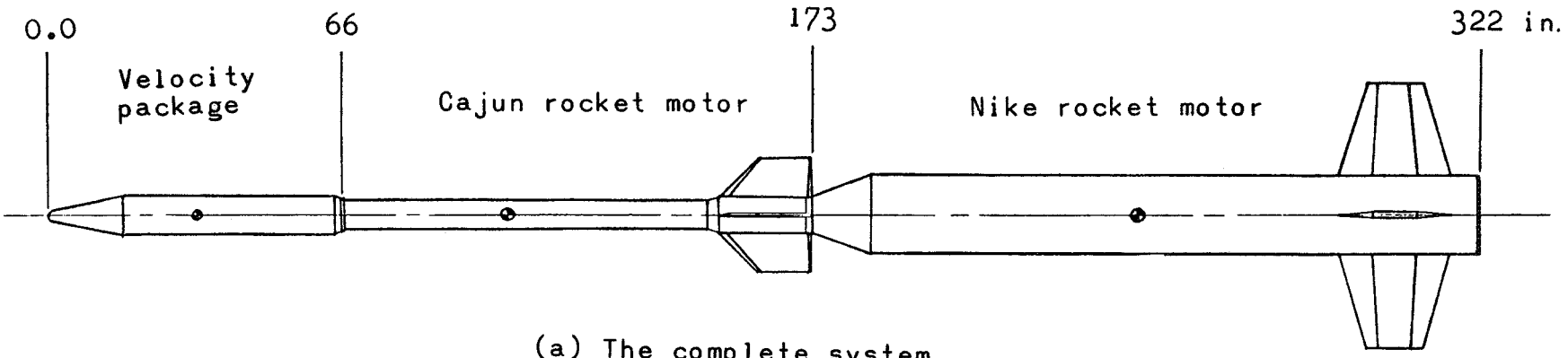

(a) The complete system

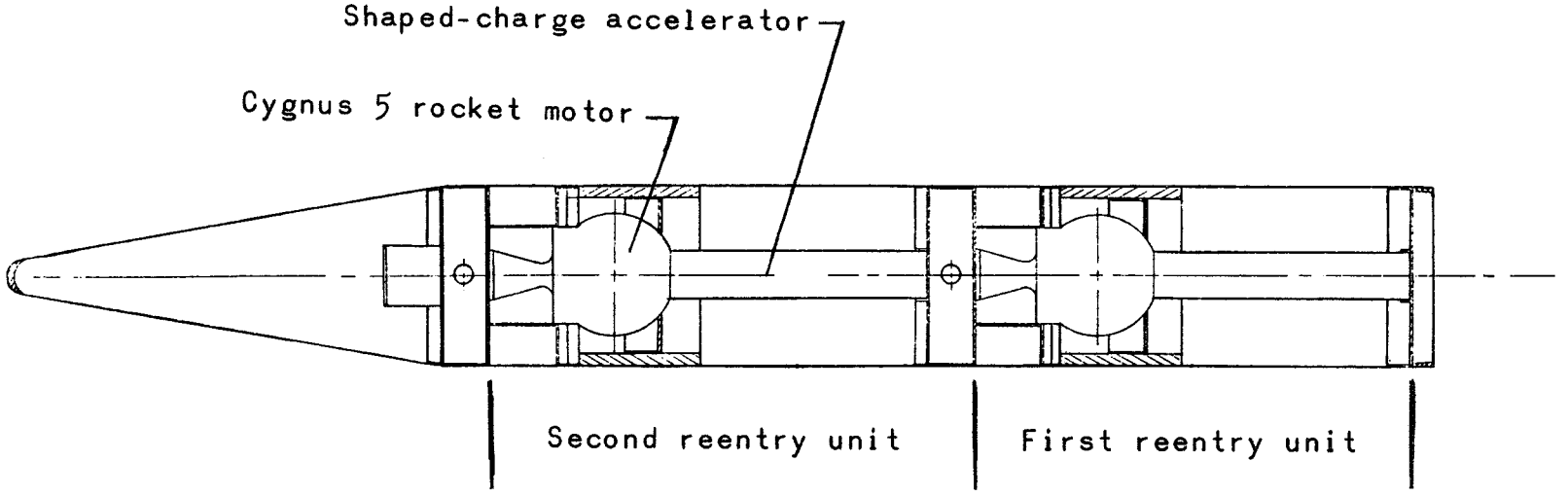

(b) The velocity package

Figure 1. The Nike-Cajun rocket vehicle system.

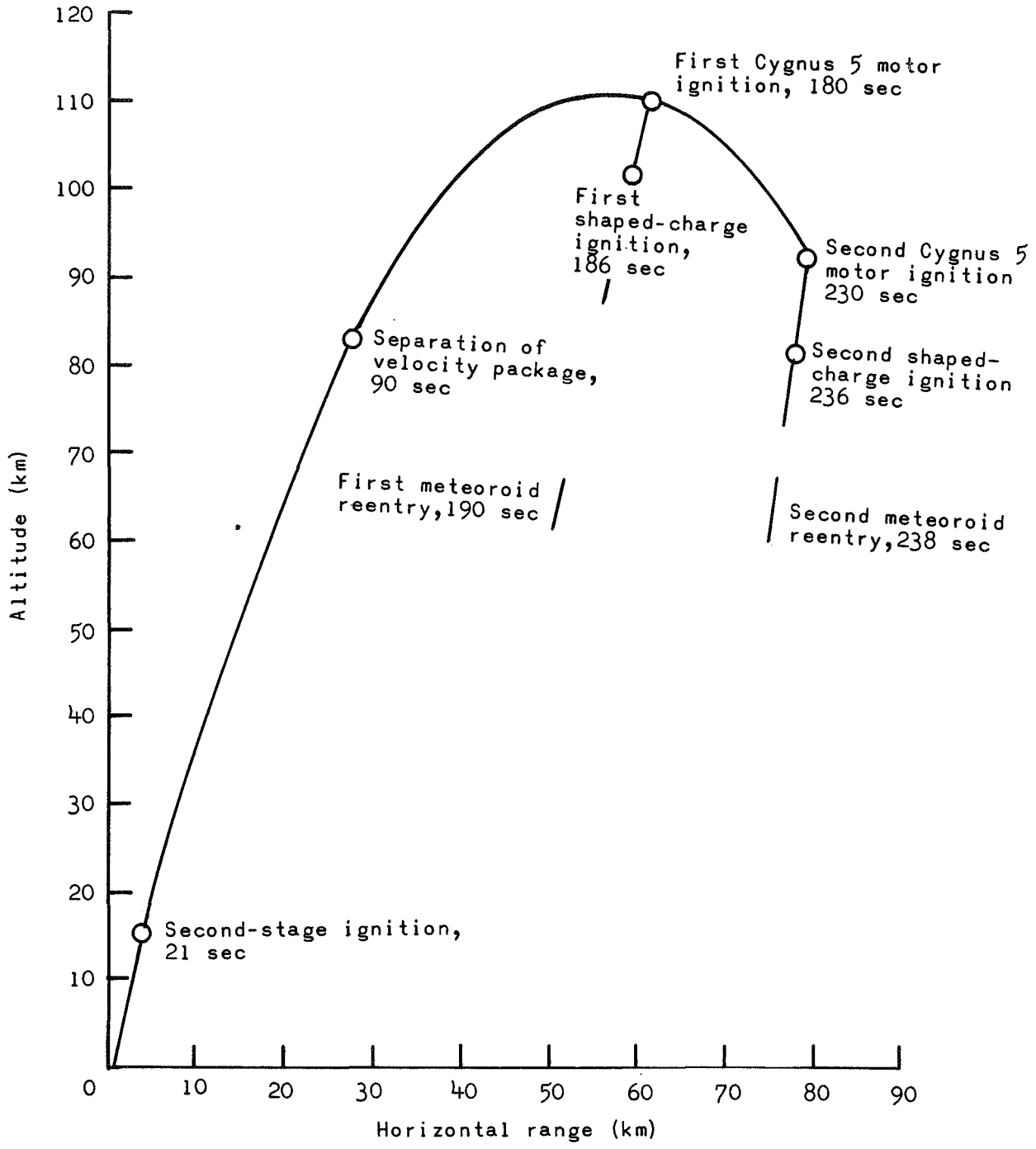

Figure 2. Nominal trajectory of a Nike-Cajun vehicle.

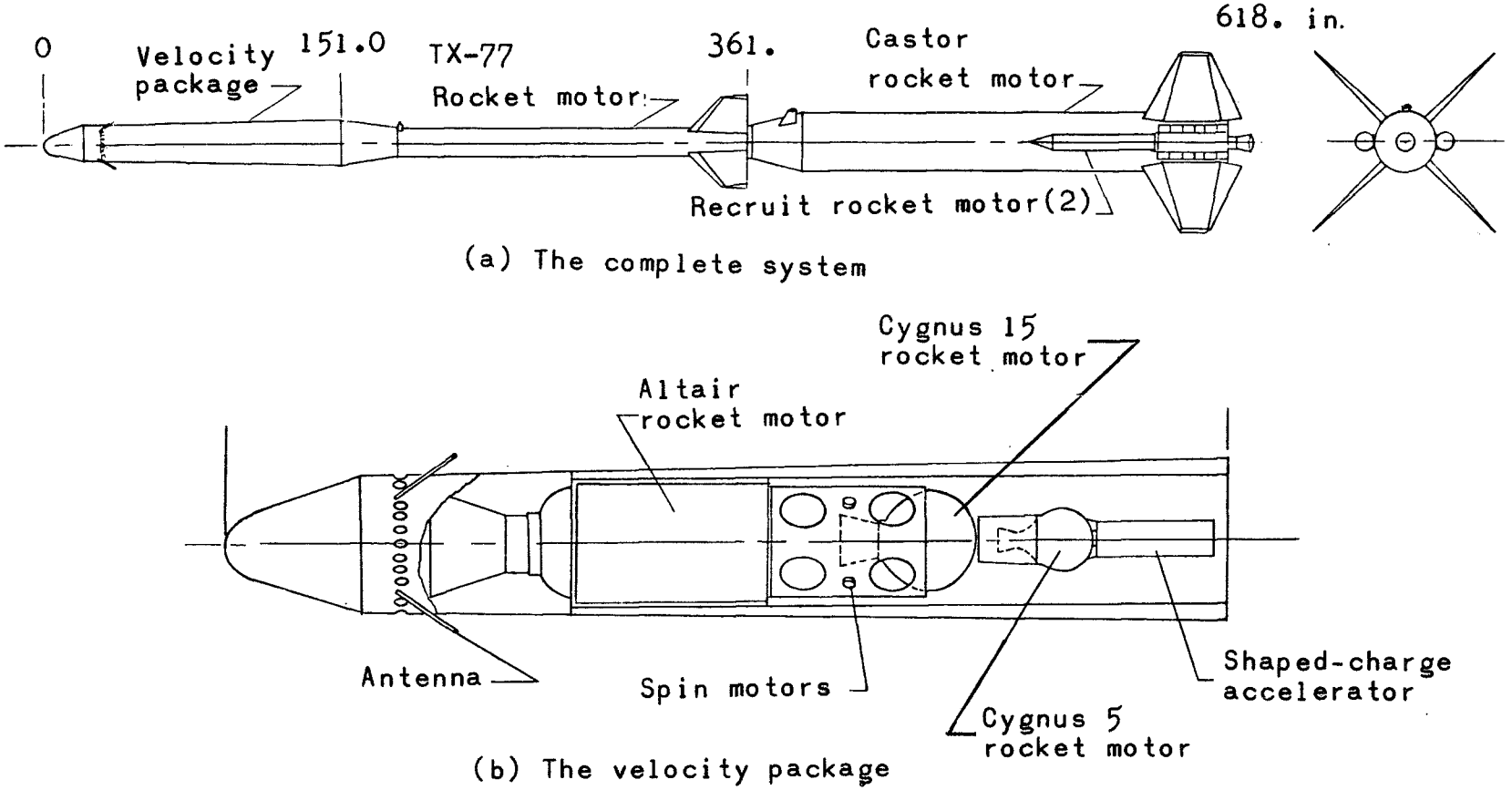

Figure 3. The Trailblazer 2 rocket vehicle system.

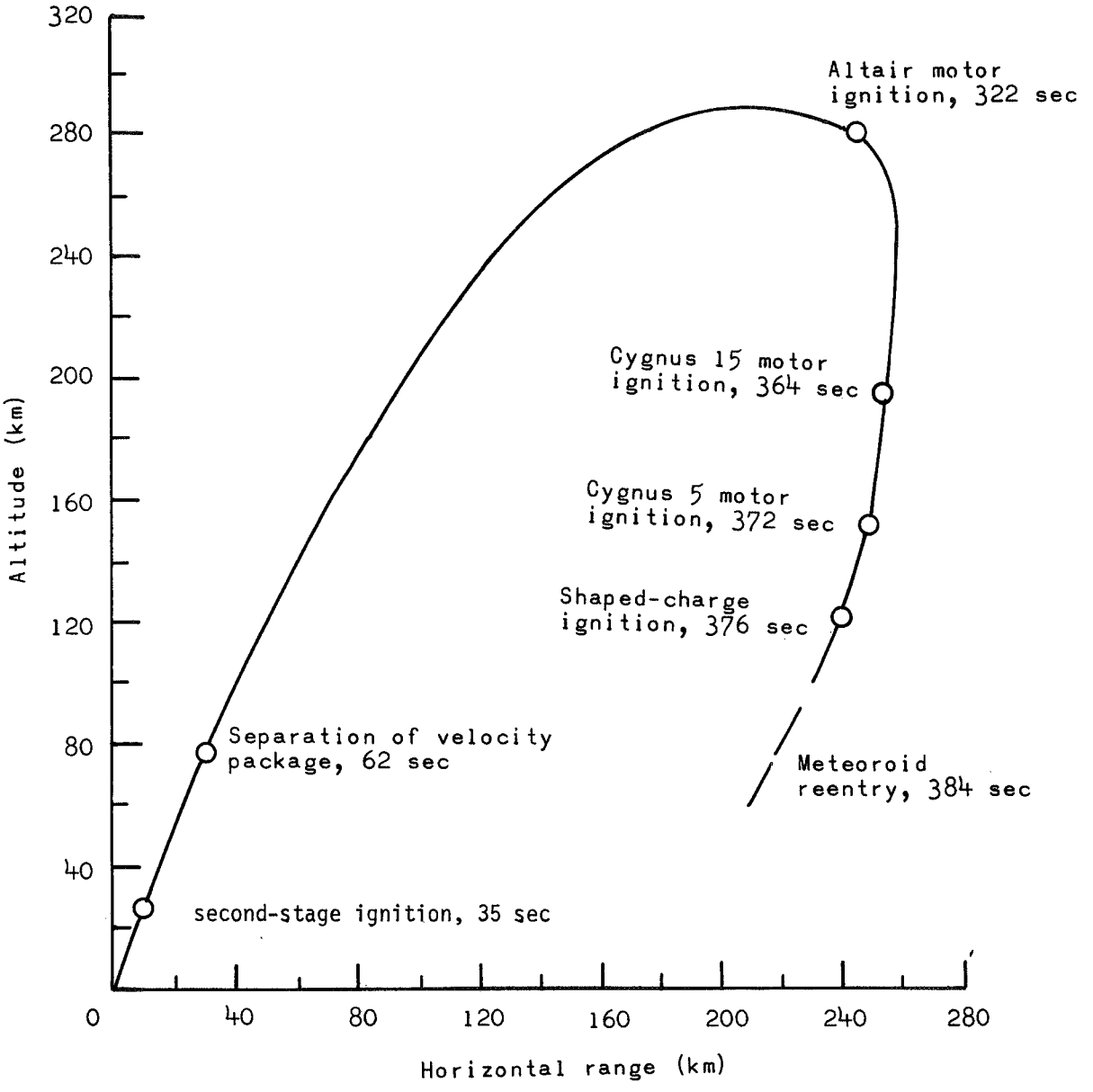

Figure 4. Nominal trajectory of a Trailblazer 2 vehicle.

The launches were carried out on dark-moon nights with good transparency for the locale. The reentry area was off the Atlantic coast to the east of the observing sites. Both NASA and SAO observers made visual and photoelectric timings of the reentries of the artificial meteors and their accelerating rockets. The predicted events for each launch were generally on schedule except for the last Nike-Cajun. For that launch, only one of the two expected reentries took place.

Table 1 gives some of the data pertinent to the experiments. Data taken from MS are included for completeness. The masses of the meteoroids given in Table 1 were determined statistically from ground test of the various types of shaped-charge accelerators used in the program.

These accelerators were of three general types. In Type I the meteoroid material was initially in the form of a disk, and in the other two types, in the form of a cone. Cross-section drawings of the three types are shown in Figure 5. Flashed x-ray photographs of the three types of artificial meteoroids taken in ground test are shown in Figure 6. Type I produced the meteoroid from a portion of a disk of ductile metal with a velocity increment of approximately 4 km sec^{-1}. At that velocity, the projectile was recoverable in ground firings. A recovered projectile is shown in Figure 7. The mass of the projectile could be accurately determined by simply weighing the recovered particle.

The Type-II accelerator produced the meteoroid from a portion of a ductile metal cone with a velocity increment of approximately 8.5 km sec^{-1}. Because of the high velocity, the projectile from this type of accelerator could not be recovered from ground firings. The masses in this instance were determined from measurements of flashed x-ray photographs. The projectiles produced by the conical type of accelerator were more irregular in shape than those produced by the disk type. Also, a larger amount of debris was associated with the production of the meteoroid. A portion of this debris traveled at nearly the same velocity as did the main particle. Under reentry conditions, the debris produced a halo of luminosity about the

Table 1. Experimental data for 10 artificial meteors.

Meteor No.	Vehicle	Accelerator	Meteoroid		Reentry	
			Material	Mass (g)	Date	Universal time
1	Trailblazer 2	Disk	Stainless steel (70% iron, 19% chromium, 9% nickel, 2% manganese)	2.2 ± 0.1	May 6, 1962	$05^h48^m26^s$
2	Nike-Cajun	Ductile cone	Iron	0.64 ± 0.16	March 12, 1964	04 20 10
3	Nike-Cajun	Ductile cone	Nickel	1.08 ± 0.32	March 12, 1964	04 20 58
4	Nike-Cajun	Brittle cone	Iron (dust)	1.5 ± 0.5	November 7, 1964	01 41 47
5	Nike-Cajun	Ductile cone	Iron	0.64 ± 0.16	November 7, 1964	01 41 55
6	Nike-Cajun	Ductile cone	Nickel	0.95 ± 0.53	May 4, 1965	05 54 01
7	Nike-Cajun	Brittle cone	Iron (dust)	1.5 ± 0.5	May 4, 1965	05 54 13
8	Trailblazer 2	Disk	1020 steel (99% iron)	5.66 ± 0.05	March 18, 1966	01 21 23
9	Nike-Cajun	Ductile cone*	Nickel	0.88 ± 0.17	September 17, 1966	02 03 17
10	Trailblazer 2	Ductile cone†	Iron	0.81 ± 0.10	February 14, 1967	05 58 20
MS	Trailblazer 1	Disk	Stainless steel (as in No. 1)	2.2 ± 0.1	April 21, 1961	06 02 00

*This is an improved version of the type of accelerator used in experiments 3 and 6.

†This is an improved version of the type of accelerator used in experiments 2 and 5.

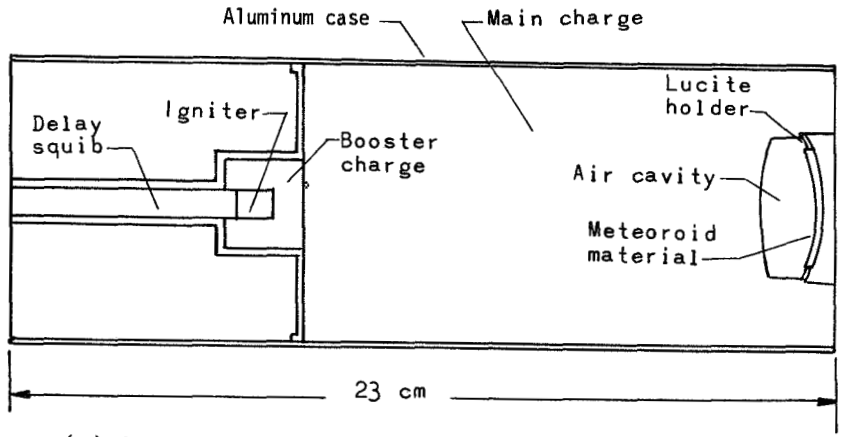

(a) Shaped-charge accelerator of the disk type (I).

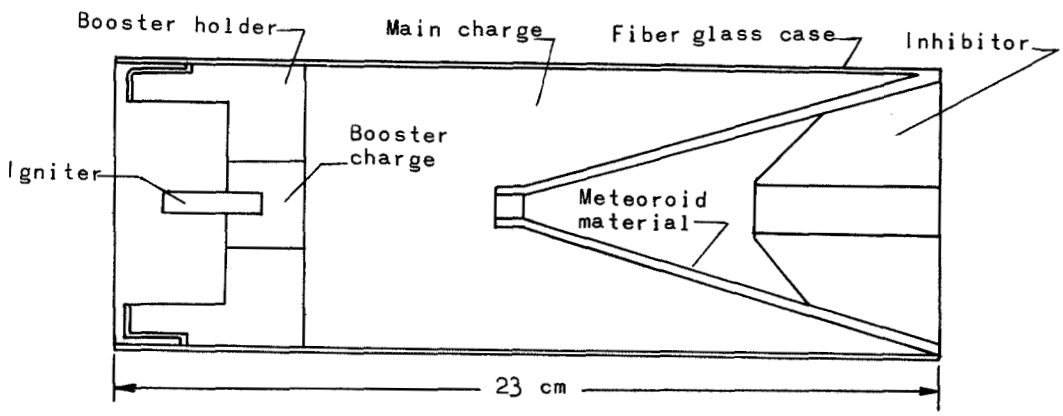

(b) Shaped-charge accelerator of the conical ductile material type (II).

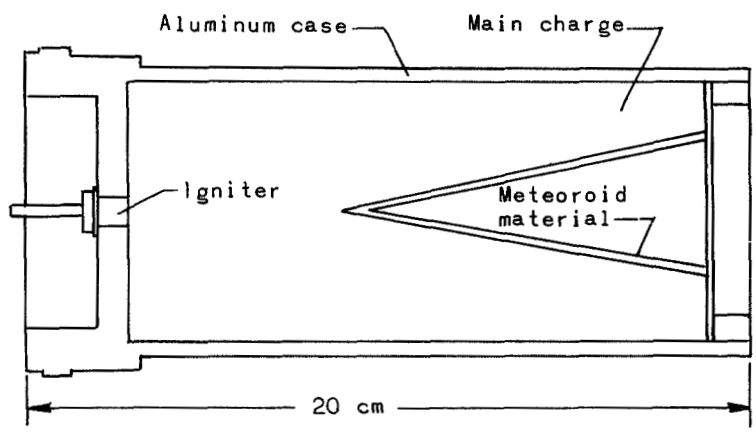

(c) Shaped-charge accelerator of the conical brittle material type (III).

Figure 5. Three types of shaped-charge accelerators used in the artificial-meteor experiments.

V = 4.3 km sec^{-1}

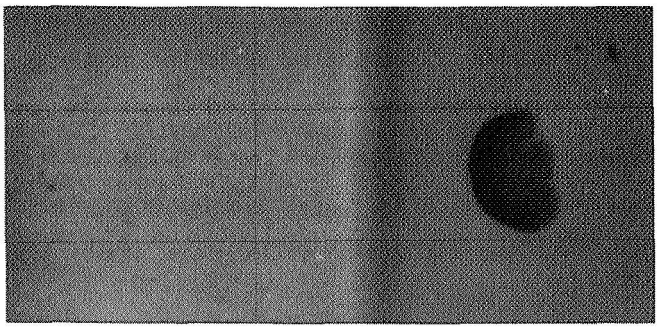

(I) Projectile from disk-type accelerator. The main projectile is formed from a major portion of the original disk. Few secondary particles are formed at the velocity of the main particle.

V = 8.5 km sec^{-1}

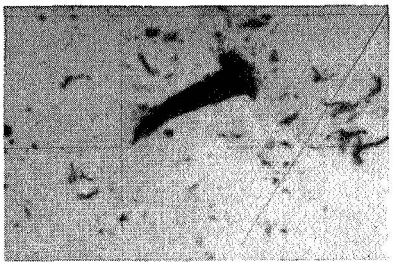

(II) Projectile from ductile cone accelerator. The main high-velocity projectile is formed from a small portion of the cone. The major portion of the cone is not accelerated to high velocities. A number of secondary particles are produced at the same velocity as the main particle.

V = 10.3 km sec^{-1}

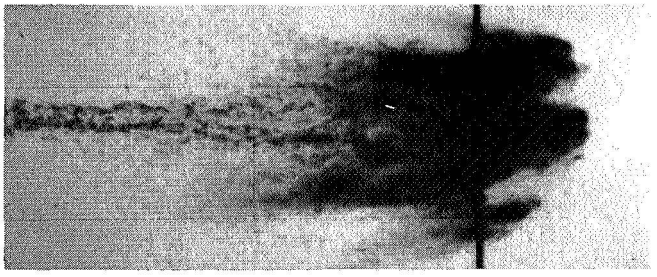

(III) Projectile from brittle cone accelerator. The projectile in this case is a fairly compact cloud of micron-size particles.

Figure 6. Flashed x-ray photographs of artificial meteoroids in ground test.

meteor and, because of differential deceleration of the fine particles, tended to obliterate the shutter breaks in the last half of the trajectory (terminal blending). Furthermore, the bulk of the luminosity usually occurred in two or more nearly equal trails, indicating that the main pellet subdivided after acceleration or that additional material had been ejected. Because of these factors, measurements of the mass of the artificial meteoroids formed by the conical accelerators are less accurate than measurements of the mass of the artificial meteoroids formed by the disk type.

The Type-III shaped-charge accelerator had a cast-iron conical liner that produced a compact cloud of micron-sized particles rather than a single large particle. The velocity increment from this type of accelerator was approximately 10 km sec^{-1}. Because of the uncertainty in the gross density of the particle cloud, the total mass of this "dust ball" could only be estimated from the flashed x-ray photographs.

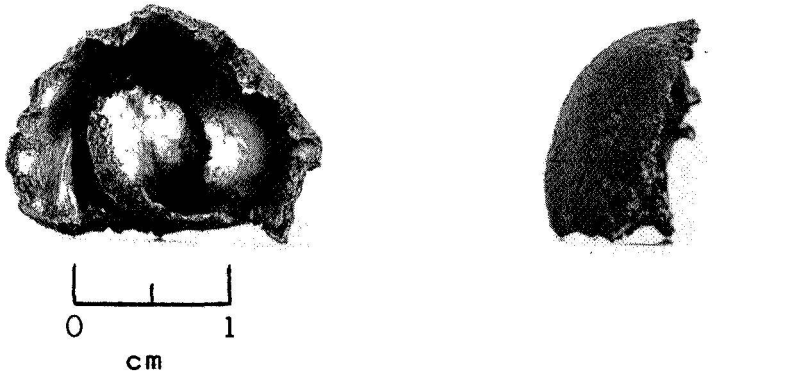

(a) Front view (b) Side view

Figure 7. Projectile recovered from ground test of Type-I accelerator.

3. OBSERVATIONS

3.1 Photographic Instrumentation

The optical characteristics of the cameras used in the observations are presented in Table 2. These cameras were located at four stations on a north-south array along the coast of Virginia and North Carolina (see Figure 8). All four stations were used in the Trailblazer experiments. The station at Coquina Beach, North Carolina, was not used for the Nike-Cajun launches.

Table 2. Camera optical characteristics.

Camera designation	Focal length (cm)	Focal ratio	Field of view
Super-Schmidt	20	0.85	57°
BC-4	30	2.6	30
K-37	30	2.5	40
K-24	18	2.5	40

Four Super-Schmidt meteor cameras were used in the observations: two at the Wallops Island station, one at Eastville, and one at Sandbridge. Blue-sensitive single-coated x-ray emulsion was the primary film for these cameras, although panchromatic emulsions were used to some extent. The camera at Eastville and one of the cameras at Wallops were equipped with focal-plane shutters for velocity measurements. In some of the later experiments, the other two cameras were equipped with Fresnel prisms for spectral measurements.

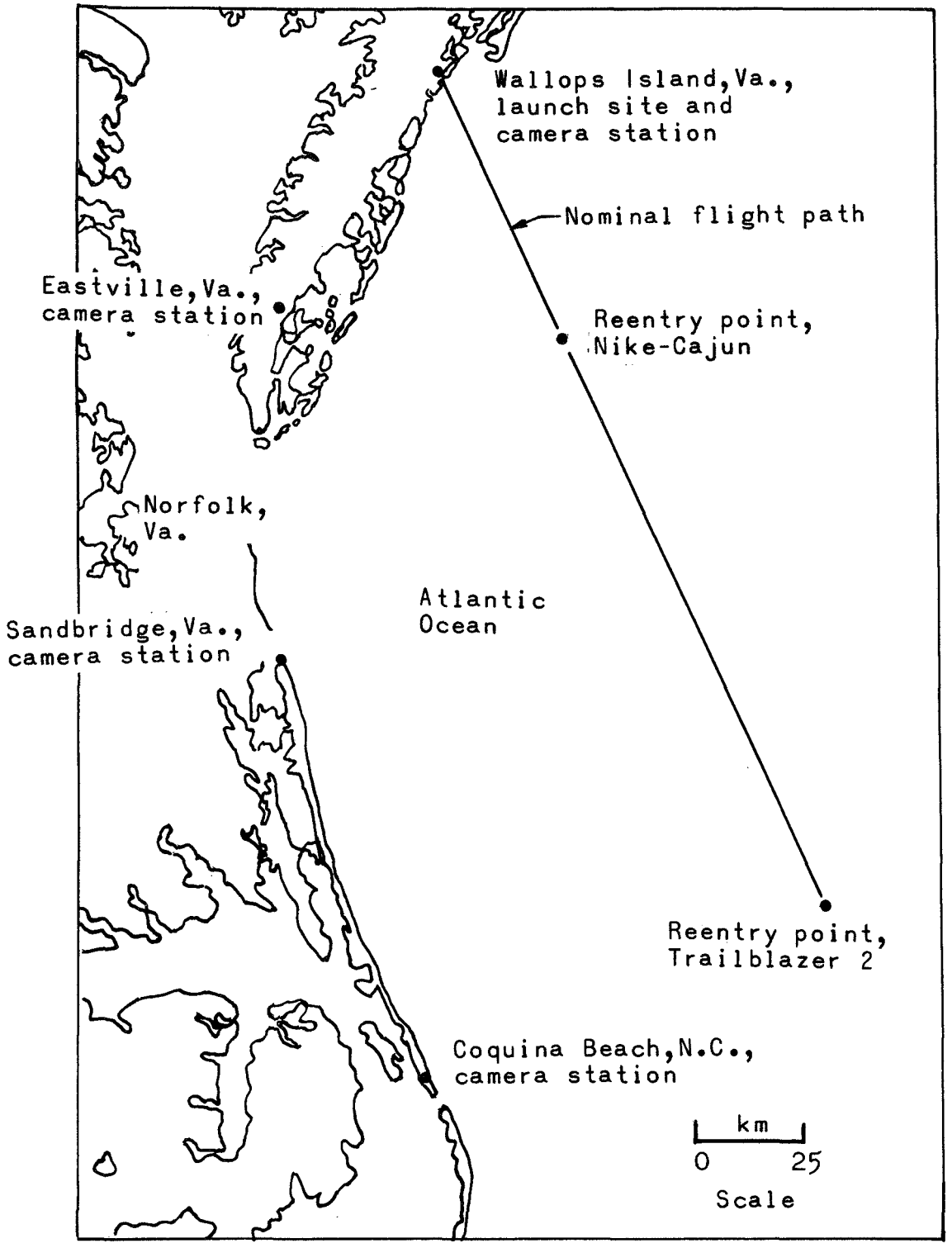

Figure 8. Map of meteor simulation test range.

The modified aerial and ballistic cameras of NASA were located at all four stations. Most of these cameras were equipped with high-speed panchromatic emulsions. The BC-4 and K-37 cameras used glass plates; the K-24 cameras used roll film.

Typical photographs of the artificial meteors taken with these cameras are presented in Figures 9 and 10.

3.2 Ballistic Data

Table 3 summarizes the key ballistic quantities for all 10 meteors. The geometric reduction for height, velocity, and zenith angle followed the precision method for photographic meteors (Whipple and Jacchia, 1957). These data were obtained primarily from photographs taken by the Super-Schmidt cameras located at Wallops (W) and Eastville (E).

The column heads in Table 3 are self-explanatory, but a few remarks may be added. In case of terminal blending, the duration of the blended portion was computed with a constant velocity from the last meaningful velocity measurement and the distance along the trail. The beginning velocity refers to the first measurable meteor dash, which usually, but not always, corresponds to the beginning height. The beginning and end heights are at the end points of the luminous trajectory. When two fragments from one meteoric body were reduced (as in the case of meteors 2 and 7) and their angular separation was small ($<2°$), mean values of the zenith distances of their midpoints and radiants (Z_R) are quoted.

In general, the meteors from the Trailblazer experiments yielded data of much higher quality than did the meteors from the Nike-Cajun experiments. The latter invariably produced meteors with multiple, blended, or diffused trails, and the data from these experiments were particularly difficult to analyze. In some cases, luminosity of the shaped-charged detonation contaminated the photographic records of the artificial meteors.

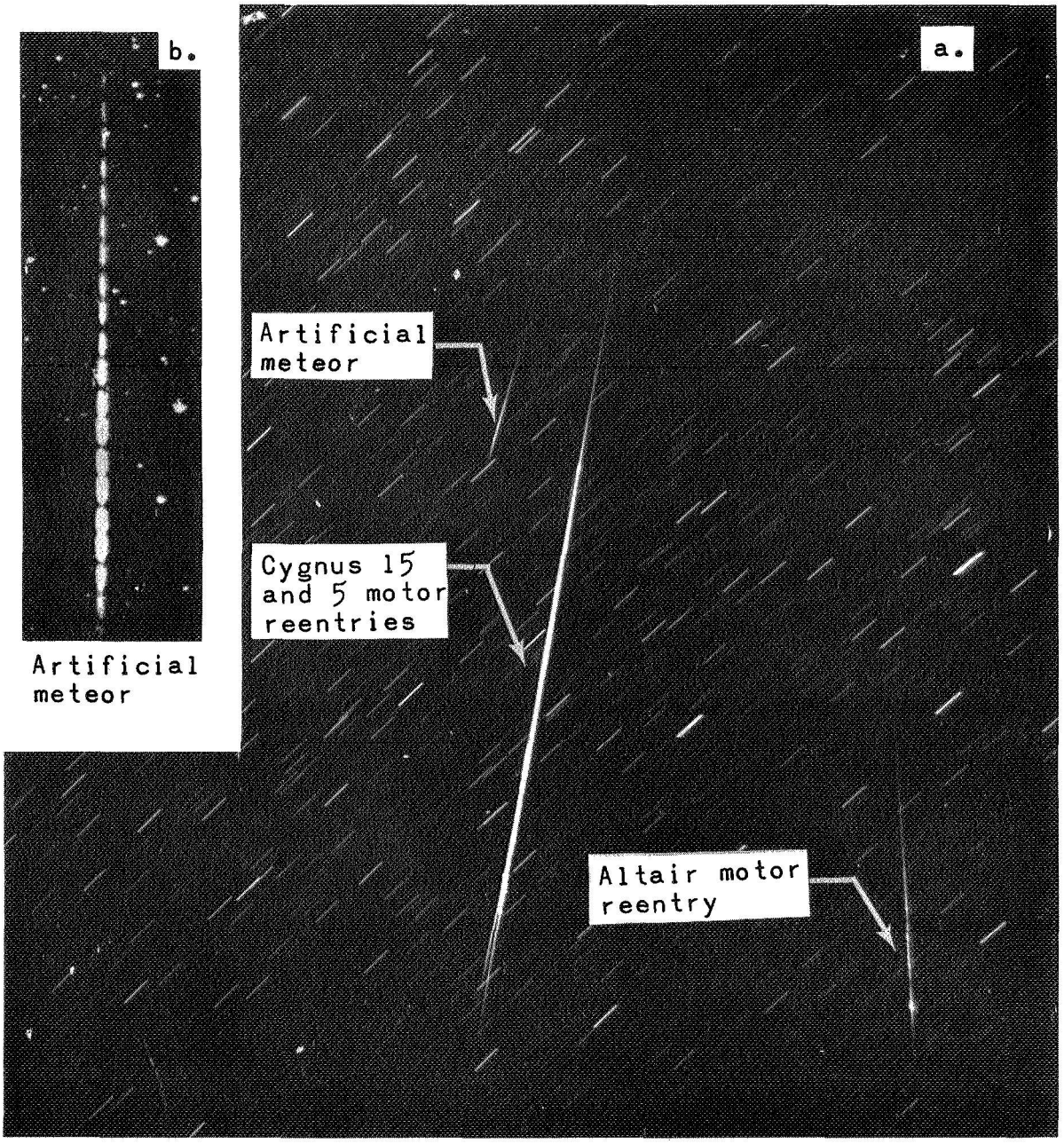

Figure 9. Photographs of an artificial meteor.

Table 3. Observational data from 10 artificial meteors.

Meteor No.	Duration (sec)	Initial velocity (km sec^{-1})	Height (km) Beginning	Height (km) End	Zenith distance at midpoint W	Zenith distance at midpoint E	Z_R	$\tau_{pg} \times 10^{12}$ (sec erg^{-1}, 0 mag)	$\tau_{pan} \times 10^{12}$ (sec erg^{-1}, 0 mag)	C.I. (see eq. (5))
1	0.8	11.9	75.9	66.2	71°	68°	22°	1.34 ± 0.29	0.80 ± 0.14	-0.56
2	2.2	9.0	80.5	64.0	33	47	9	2.5 ± 1.0	0.79 ± 0.36	-0.86
3 (Ni)	1.5	8.5	74.1	62.9	44	51	27	0.14 ± 0.06	—	—
4	0.2	11.0	68.8	67.5	58	54	20	1.1 ± 0.7	1.7 ± 1.0	+0.47
5	0.4	9.6	62.0	60.7	62	58	15	2.0 ± 0.6	0.87 ± 0.26	-0.90
6 (Ni)	1.2	10.1	78.2	66.9	43	44	20	0.46 ± 0.17	—	—
7	0.6	11.0	80.4	74.6	48	45	23	1.3 ± 0.5	1.4 ± 0.5	+0.08
8	1.0	10.9	71.1	60.5	73	69	23	0.89 ± 0.09	0.61 ± 0.08	-0.41
9 (Ni)	1.4	11.4	81.4	66.7	31	39	21	0.99 ± 0.23	0.49 ± 0.11	-0.76
10	1.0	16.4	84.9	73.7	75	72	17	1.81 ± 0.34	1.04 ± 0.2	-0.60
MS	0.8	9.8	69.4	62.6	76	—	15	0.8	—	—

NOTES:

Meteor No. 1 – A difference of nearly one magnitude exists in the light curves derived from the two Super-Schmidt films. This greatly exceeds a probable error of photometry. Both the color index and a comparison of the shapes of the light curves with the panchromatic results indicate that the data from Station E is superior and we have therefore rejected Station W data.

Meteor No. 2 – The photometry of the panchromatic film includes only the brightest trail. The tabulated color index is computed on the assumption that this trail, as in the case of the photographic data, represents 70% of the total luminosity.

Meteors No. 3, 4, 5, and 7 – Accurate velocity histories are not available, and constant velocities have been assumed in deriving τ.

Meteor No. 10 – Photoelectric observations of this meteor show that it was luminous for about 0.6 sec before it was photographed on the panchromatic film. A linear extrapolation of the light curve to a time of -0.4 sec (see Figure 20) increases τ by about 20%.

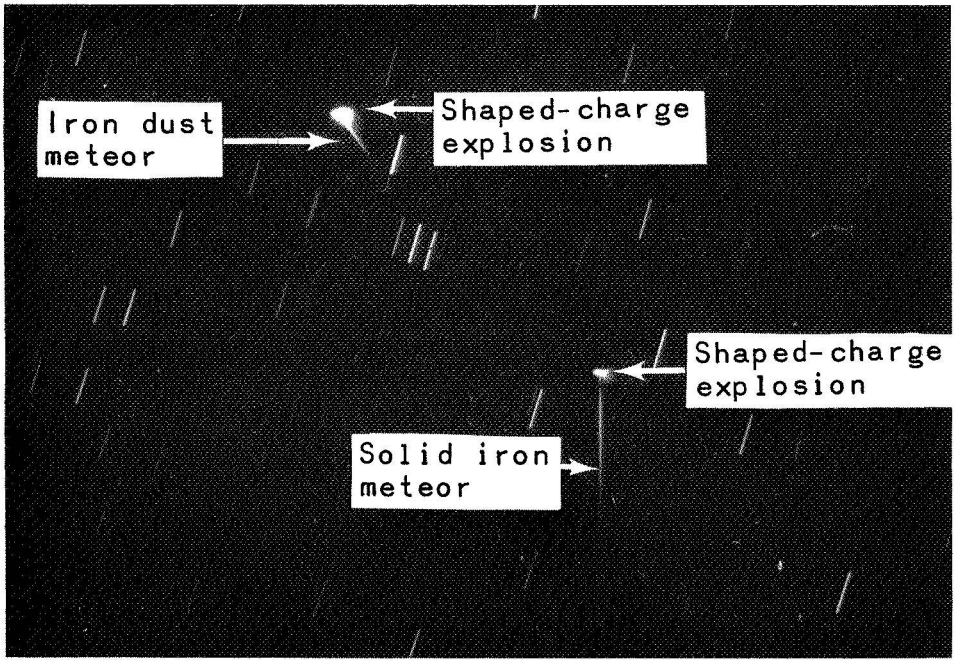

Figure 10. Ballistic camera photograph of the reentry phenomena of a Nike-Cajun experiment.

The following is a brief description of each artificial meteor:

Meteor 1. This was a good meteor, with no blending of the trail. Velocity measurements were possible over the complete trail.

Meteor 2. This meteor was characterized by multiple reentries and blending. Velocity measurements were possible only on the central one-third of the trail.

Meteor 3. This very faint meteor was recorded only by the Super-Schmidt cameras. Velocity measurements were poor because of blending of the trail.

Meteor 4. The shaped-charge accelerator detonated at an altitude of 69 km. The meteor trail was less than 2 km long and displayed considerable lateral dispersion. The trail was partially obscured near peak light by the shaped-charge detonation. Velocity measurements were possible for the first one-half of the trail not obscured by the explosive flash.

Meteor 5. The shaped-charge accelerator detonated at an altitude of 62 km. The meteor trail was less than 2 km long. A small portion of the trail was obscured by the flash. There was considerable blending. Velocity measurements were possible only on the first one-third of the trail.

Meteor 6. This nickel meteoroid fragmented into two major and several minor objects. The two major fragments produced faint meteors of nearly the same brightness, velocity, and duration. Velocity measurements were possible for approximately two-thirds of each main trail. The Super-Schmidt cameras were the only ones to photograph this event.

Meteor 7. The shaped-charge accelerator that produced this iron dust meteor was detonated at an altitude of 81 km. The meteor trail showed some lateral dispersion and blending. The shaped-charge detonation obscured a small portion of the trail. Velocity measurements were possible for the first half of the trail.

Meteor 8. This was a good meteor with no blending or dispersion of the trail. Velocity measurements were possible over the complete trail.

Meteor 9. This was the best of the nickel meteors. There was one main bright trail with several much dimmer and shorter ones. The main trail showed very little blending. Velocity measurements were possible over all of the main trail.

Meteor 10. This was a good meteor and showed no blending nor dispersion of the trail. Velocity measurements were possible over the complete trail.

3.3 Photometric Data

Mean light curves for the 10 artificial meteors are given in Figures 11 through 20. In most cases, the curves are the average of two or more light curves obtained from cameras located at different stations. An estimate of error for each curve is given by an error bar at peak light.

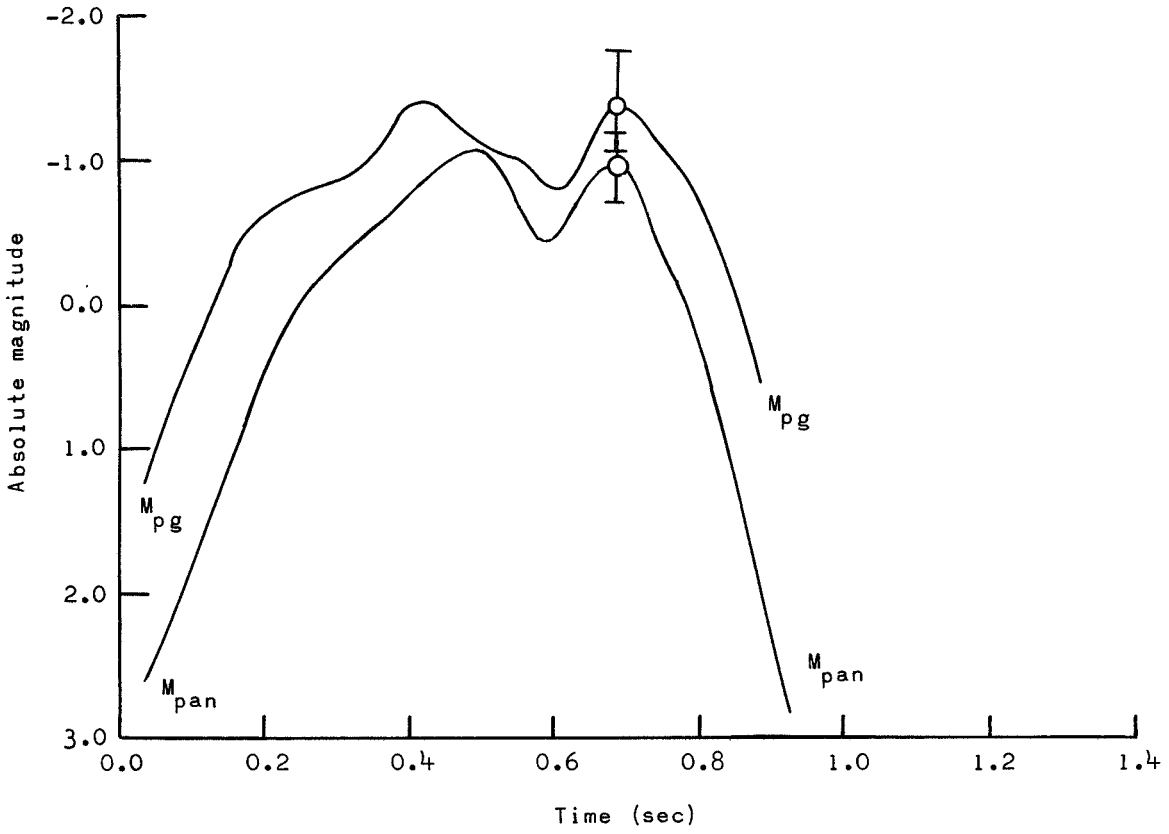

Figure 11. Light curves for meteor 1.

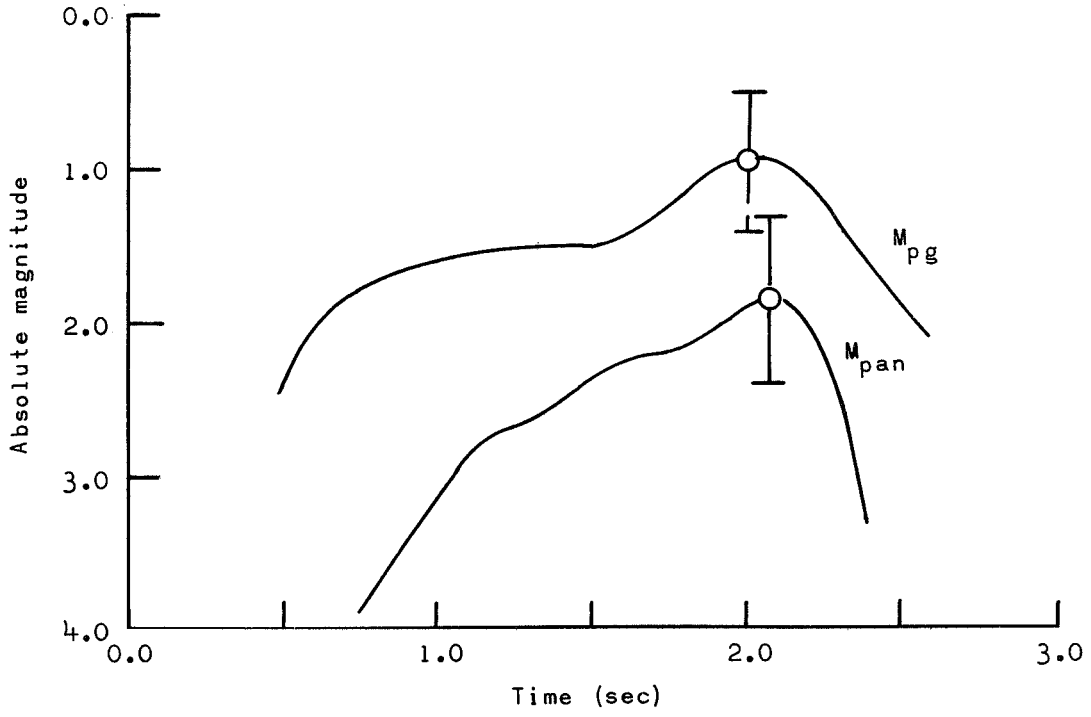

Figure 12. Light curves for meteor 2.

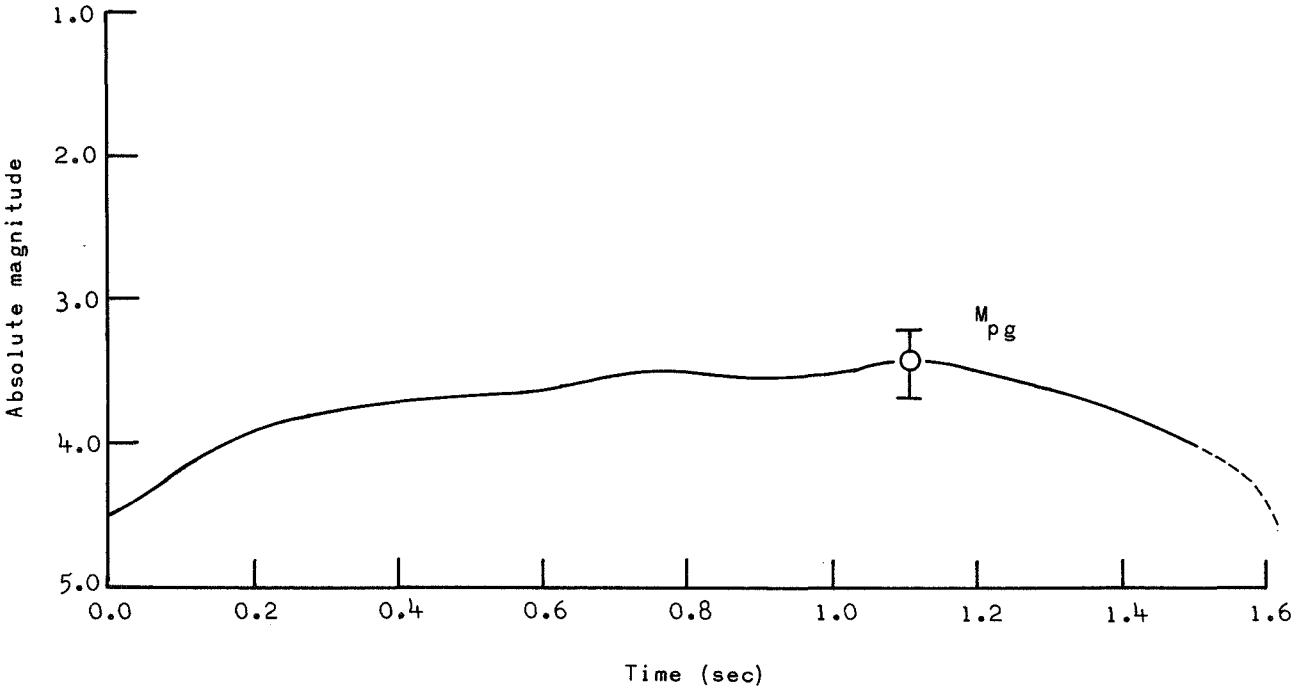

Figure 13. Light curve for meteor 3.

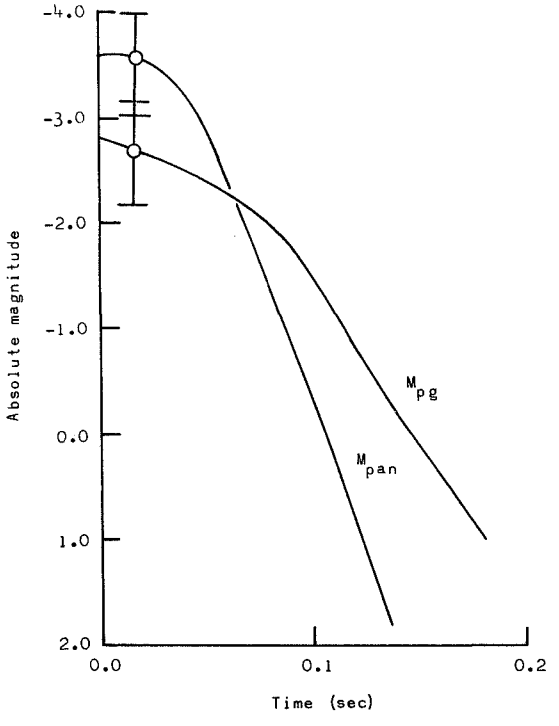

Figure 14. Light curves for meteor 4.

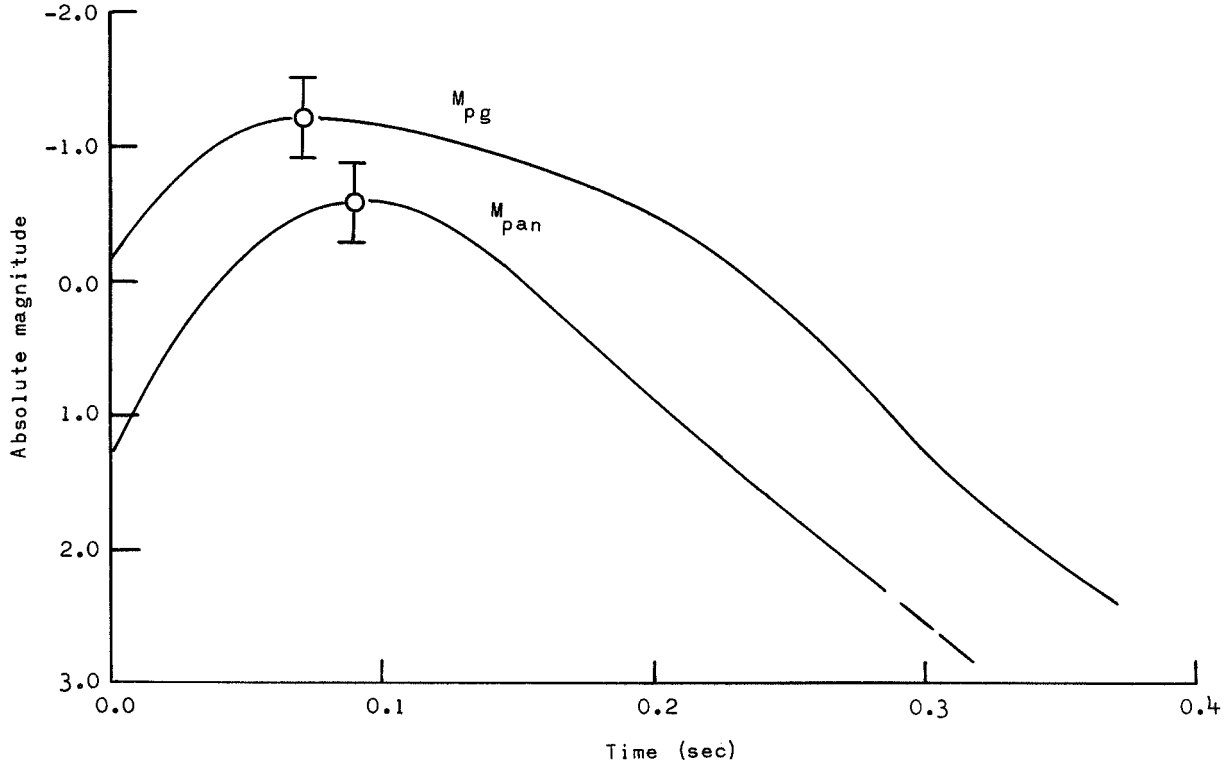

Figure 15. Light curves for meteor 5.

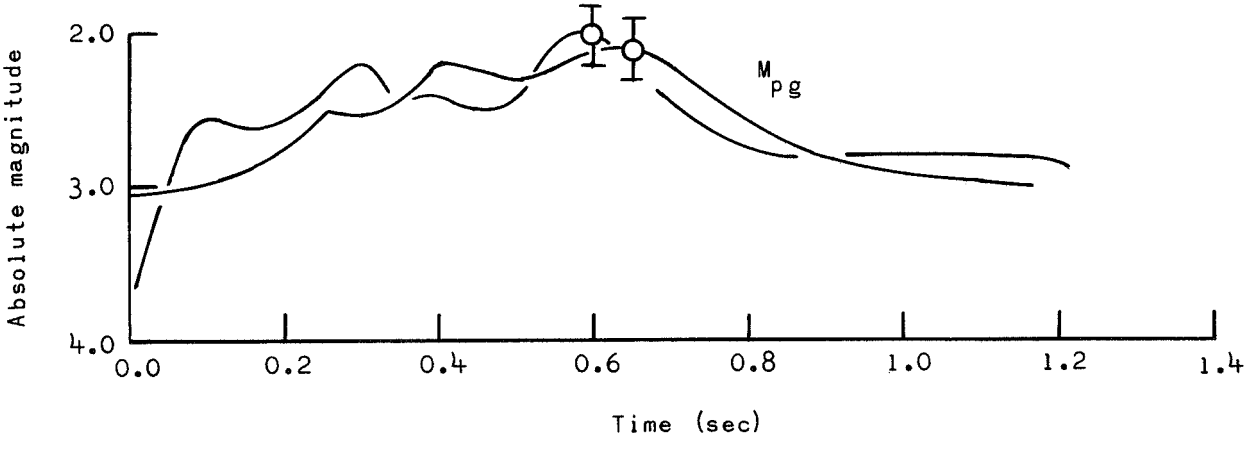

Figure 16. Light curves for meteor 6.

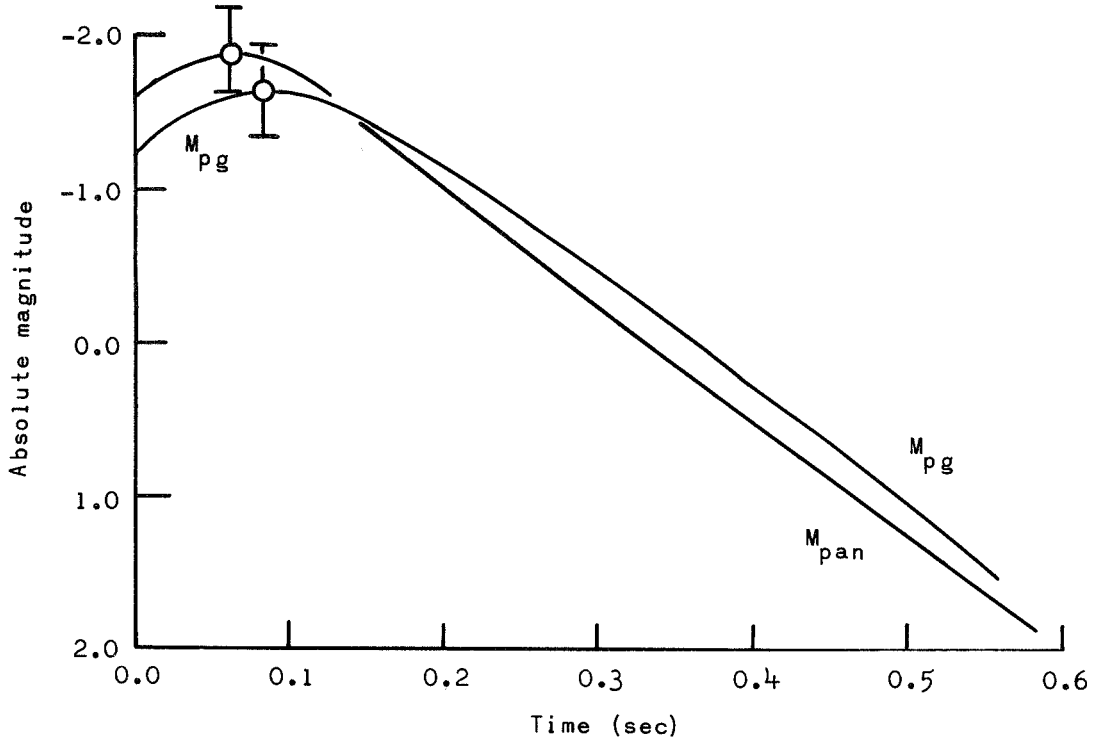

Figure 17. Light curves for meteor 7.

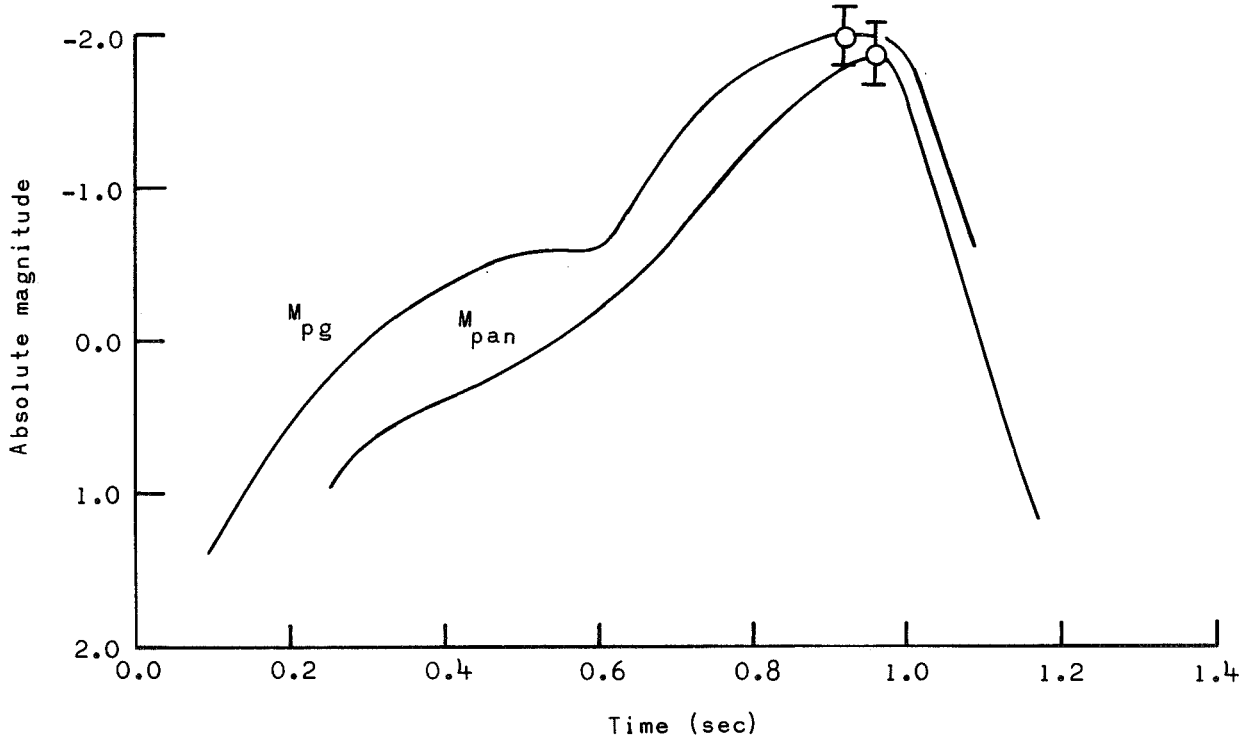

Figure 18. Light curves for meteor 8.

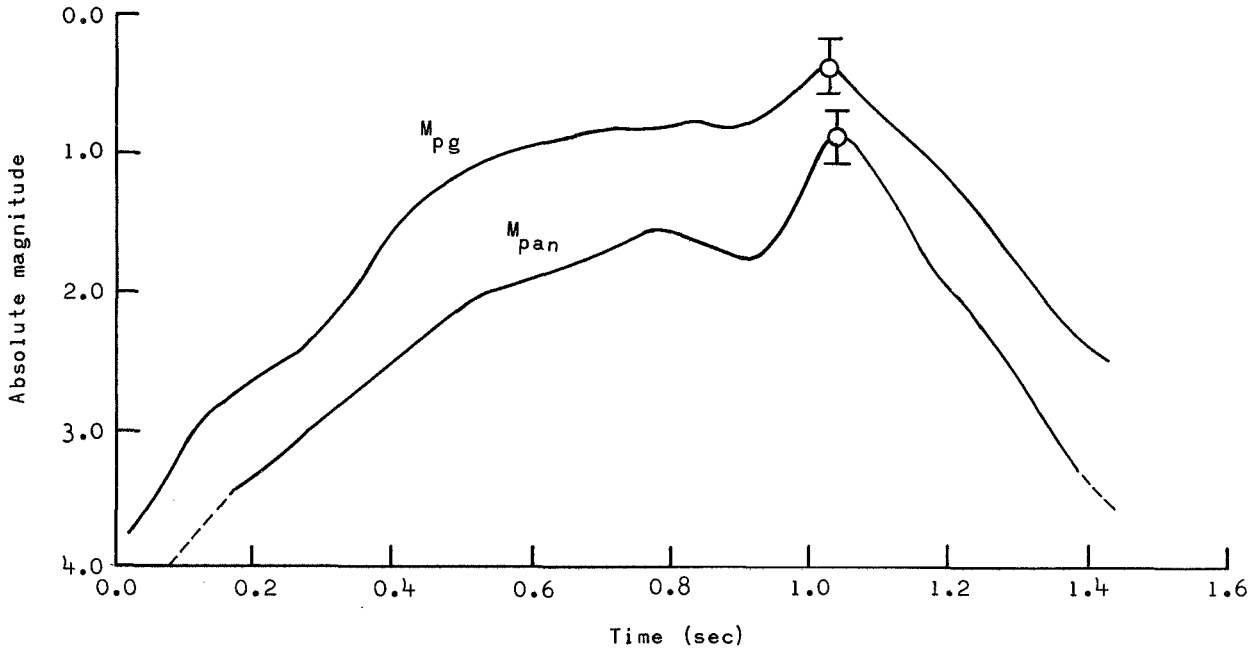

Figure 19. Light curves for meteor 9.

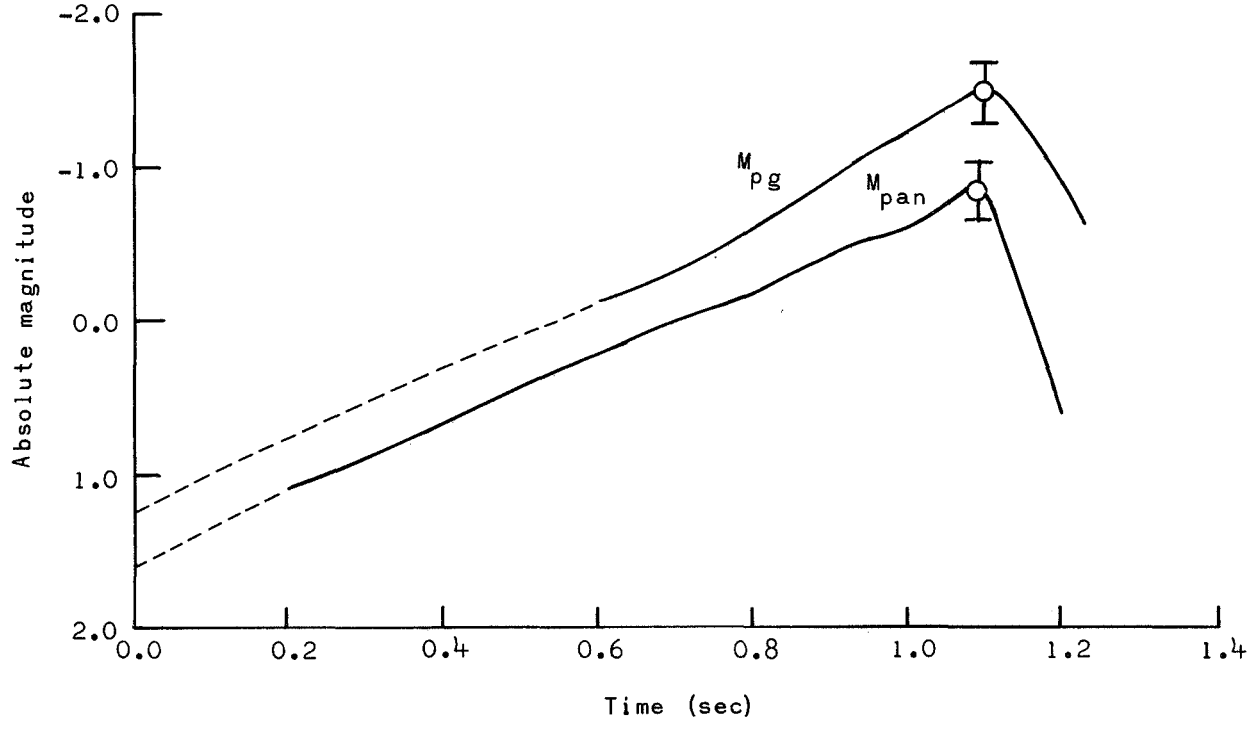

Figure 20. Light curves for meteor 10.

All the photographic (blue-sensitive) light curves labeled M_{pg} in the figures and the panchromatic curve labeled M_{pan} for the nickel meteor 9 are from the Super-Schmidt photographs. The panchromatic light curves for the iron meteors are from the NASA camera photographs.

The photometric analysis of the Super-Schmidt photographs was performed at SAO, and that of the NASA camera photographs, at LRC. In both cases, the analyses followed the general techniques described by Jacchia (1949). However, there were significant differences in the details of the data reduction conducted at the two centers. In the SAO method, the meteor trail images were compared visually with trailed star images on photographs different from the meteor photographs. A discussion of the SAO method is presented in Appendix A. In the NASA method, microphotometer traces of the meteor trail image were compared with similar traces of trailed star images located near the meteor and on the same photograph as the meteor. The NASA method is described by Ayers (1968).

The two methods generally produced similarly shaped light curves for the individual meteors, suggesting that there is no radical differential change in the luminosity for $\lambda < 5000$ Å as compared to $\lambda > 5000$ Å. The tendency for the panchromatic light curves to have steeper slopes at the beginning and end of the trajectory — where photometry is more difficult — is, we believe, more likely to be a systematic error in one or both methods of photometry rather than a physical effect.

Except for the dust-ball meteors, Nos. 4 and 7, the photographic magnitudes at maximum light are less than the panchromatic values. We have already noted the difficulty in distinguishing the meteor from the shaped-charge explosion for those two meteors. Increased red emission in the explosion gases may produce a panchromatic enhancement that we have attributed to the meteor phenomena. If so, we have overestimated the luminosity due to these two meteors.

4. LUMINOUS EFFICIENCY AND COLOR INDEX

The luminous equation for meteor intensity I is given by

$$I = -\frac{1}{2}\,\tau V^2\,\frac{dm}{dt} \quad , \tag{1}$$

where τ is the luminous efficiency factor, V is the velocity, and m is the mass. Thus,

$$\tau = \frac{2}{m}\int_0^T \frac{I}{V^2}\,dt \quad , \tag{2}$$

where T is the observed duration of a meteor. Since the values of I and V can be obtained directly from the observational data and since m is known for the artificial meteors (Table 1), equation (2) enables us to calculate τ.

The instantaneous meteor intensities were taken from the mean light curve for each meteor from the relation

$$M = -2.5 \log I \quad . \tag{3}$$

By numerical integration of equation (2), we computed the value of τ in terms of cgs units and a zero-magnitude star, M_{pg}. Extrapolated regions of the light curve (Figures 11 to 20) indicated by dashed lines were included in the integration. The results are given in columns 8 and 9 of Table 3 for the photographic (pg) and the panchromatic (pan) luminous efficiencies (τ). In some cases (see Notes to Table 3), when trail blending prevented a determination of the velocity history of the pellet, a constant velocity equal to the initial velocity was assumed. In this event, τ might be underestimated by as much as 10%.

The data are very inhomogeneous with regard to their quality and should not be mixed indiscriminately. We will first discuss the three Type I and one Type II projectile experiments that produced single trails without blending and then compare the other results with these superior data.

Color indices of meteors are generally expressed as a comparison of maximum light observed photographically and visually, i. e.,

$$\text{C. I. (pg, v)} = M_{pg} - M_{v} \quad . \tag{4}$$

Large observational errors in the visual estimates restrict the use of the color index to statistical samples of meteors (Jacchia, 1957). With the present small sample of accurate data, a color index defined by the integrated luminosity seems more appropriate since it avoids the vicissitudes of photometry at a single point. Except for minor changes in velocity along the luminous trajectory, the integrated intensity is proportional to the computed values of τ. We then define

$$\text{C. I. (pg, pan)} = -2.5 \log \frac{\tau_{pg}}{\tau_{pan}} \quad . \tag{5}$$

The values are given in Table 3. The mean value for events 1, 8, and 10 is

$$\text{C. I. (pg, pan)} = -0.52 \quad . \tag{6}$$

Ayers (1968) finds that <u>stars</u> photographed by the panchromatic detection system follow the approximate relationship

$$\text{C. I. (pg, pan)} = 0.38 \text{ C. I. (pg, v)} \quad . \tag{7}$$

If we apply this formal relationship to the color index observed for the artificial meteors, we obtain C. I. (pg, v) = -1. 4, in good agreement with Jacchia's determination of C. I. (pg, v) $\approx$ -1. 5 for natural meteors. The importance of the similarity should not be overemphasized since it is derived under the questionable assumption that the spectral distribution of the meteor,

an emission line source, can be compared with an approximate blackbody source such as a star. Nevertheless, since the observations of both sets of objects in the three detection systems (photographic, visual, and panchromatic) extend over such a broad and overlapping spectral range, it would have been surprising if there were not a reasonable agreement between the two methods of color determination. We accept the agreement as an indication that large systematic errors are unlikely in the color-index data of either the artificial or the natural meteors.

4.1 Velocity Dependence

The data show a clear trend of increasing τ_{pg} with increasing velocity. Combining the results of the four unblended meteors, including meteor MS, in a least-squares solution of the form

$$\log \tau = a + n \log V \quad , \tag{8}$$

we find

$$n = 1.9 \pm 0.4 \quad ,$$

where the quoted error is the standard deviation. If, on the other hand, we accept from natural-meteor observation that $n = 1$ and that

$$\tau = \tau_0 V \quad , \tag{10}$$

where τ_0, the luminosity coefficient, is a constant, then

$$\log \tau_0 = -18.03 \pm 0.07$$

in cgs units and zero magnitude. This can be compared with $\log \tau_0 = -18.1$ determined from the MS experiment alone.

The corresponding value for the panchromatic observations of meteors 1, 8, and 10, on the assumption that the color index is -0.52 and independent of velocity, is $\log \tau_{0_{pan}} = -18.22$.

The remaining Type-II iron accelerators, events 2 and 5, both produced multiple and blended trails that made photometry and velocity determination difficult. In addition, meteor 5 was launched at an unplanned low altitude, and the trail is confused by the shaped-charge explosion. The color index of both trails is consistent with that of the Type-I events, but the total luminosity exceeds by factors of 3 to 5 that expected from extrapolation of the Type-I events. We think it unlikely that errors in the photometry are responsible for any discrepancy beyond a factor of 1.5. It is certain, from the photographic evidence, that much of the debris produced by the shaped charge entered with the major pellet(s). We believe that an underestimate of the effective mass of these objects is the primary cause of the discrepancy. The remaining possibilities are the following: 1) Type-I single-body objects are less efficient light producers, possibly because they have a larger fractional terminal mass than the smaller fragments of Type II or 2) the luminous efficiency in fact increases again at the lower velocities at which these objects reentered. Results of Type-III events discussed below suggest that the first possibility is unlikely. The second is implausible on the face of it, and, if true, would require that this remarkable behavior occurred abruptly between 9.6 and 9.8 km sec^{-1} (the lowest velocity obtained with a Type-I accelerator).

The Type-III dust-ball accelerator events (4 and 7) show a slight positive color index. We suppose this to be due to a more severe contamination of the meteor in the red region of the spectrum by the explosion gases. In Figures 14 and 17 the panchromatic intensities exceed the photographic only during that first portion of the meteor adjacent to the shaped-charge explosion. The photographic luminous efficiency exceeds that of Type-I experiments by about 50%. The uncertainty in the mass (33%) and that in the photometry of these short, broad trails (50%), together with a contamination of the explosion in the blue region, are more than sufficient to explain the discrepancy.

The data for nickel are both sparse and weak but they do suggest a behavior different from that of iron in the meteoric process. A color index is available from only one meteor (event 9: C. I. (pg, pan) = -0. 8), slightly smaller than the mean value for iron.

All the nickel events (3, 6, and 9) show multiple trails or blending. Since it is easier to launch an integral pellet of nickel than one of iron, the occurrence of these phenomena indicates to us that the main mass is also accompanied by debris. By analogy with the results of the iron experiments 2 and 5, we suspect that the effective mass of the meteoroids may be larger than the masses quoted for the main pellet and that the luminous efficiencies are overestimated. If we compare results from Type-II nickel and iron experiments, we find that the luminous efficiency of nickel is about 1/3 that of iron at $V \approx 10$ km sec^{-1}.

The velocity range in the nickel experiments was small, and any determinations of velocity dependence of τ may be questioned. The best fit to the tabulated data gives $n \approx 6$ in equation (8) (see Figure 21). Blending is most severe on the low-velocity events 3 and 6. If the errors in effective mass are larger for these than for meteor 9, then the velocity exponent n given above is a lower limit.

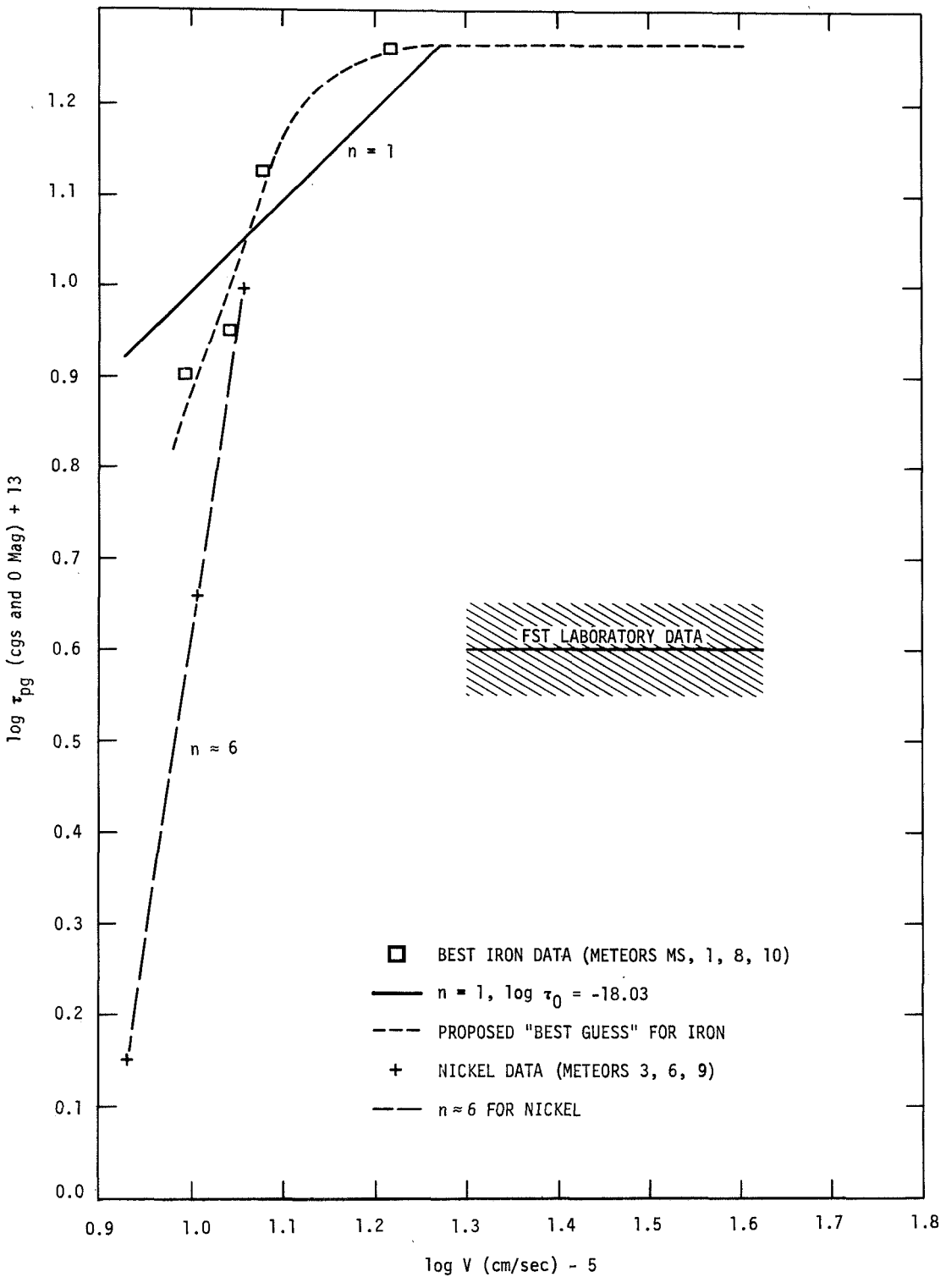

Figure 21. The luminous efficiency of iron as a function of meteor velocity.

5. DISCUSSION AND CONCLUSIONS

FST have observed the luminosity of iron particles of submicron diameters with velocities from about 20 to 40 km sec^{-1}. They obtained broad-band spectral data on some of their experiments. Using the observed spectral distribution of a particular natural meteor, they were able to make a rough conversion of their luminosity measures to the photographic system. They determined that

$$\tau_{pg}(Fe) = 4 \times 10^{-13}$$

and is independent of velocity. When this result was compared with that from the artificial meteor data then available (meteor MS), a factor of 2 discrepancy was noted. Considering the difficulty of both experiments, this was properly judged to be reasonable agreement. With the addition of the new data presented here, the discrepancy between the two determinations has increased to a disturbing factor of 4 or more (see Figure 21). We cannot conceive of a physical cause that would produce a rapid decrease in the luminous efficiency in the unobserved velocity range $16 < V < 20$ km sec^{-1}. The disparate results must certainly be due to errors in one or both of the experiments or to important physical differences between them. The laboratory experiments appear to us to have been exceedingly well controlled, especially so when compared with the artificial meteors. We do not think the answer lies in that direction. The artificial-meteor results depend both on the assumption concerning the relative luminous efficiencies of iron to other elements present in the pellet (for events MS and 1) and on the actual mass entering into the light production. Composition effects, as discussed by MS, are too small to produce the discrepancy. In events 8 and 10 there are no compositional differences.

Type-I accelerators produce the most reliable masses. The absence of any visible debris or blending confirms that a single pellet was responsible for the great majority of the light. The preacceleration mass of the pellet for meteors MS and 1 is less than three times the mass of that part assumed to have reentered. This sets an absolute limit to the correction that can be applied to reduce the luminous efficiency by a mass error. No ground tests of the accelerator show the mass error to exceed 1.2. The improved ductile cone accelerator used for event 10 does not have the same reliability as the Type-I accelerator, but the optical evidence strongly suggests that the particular device used behaved in a nominal manner. Debris and blending are absent, and we believe the datum obtained from this flight is valid. If we ignore it, we still remain with a discrepancy of about a factor of 3 between the laboratory work and the flight experiment.

Finally, following the justifications given by MS, we assume that all the mass is consumed in the meteor process. Our results therefore are lower limits of the luminous efficiency. Any terminal mass effect will be more important at low velocity. A correction for terminal mass may change the velocity dependence toward that suggested by the laboratory experiments, but at the expense of an increased discrepancy in the values of τ_{pg}.

We conclude that substantial physical differences exist in the light-production process in the two types of experiments. FST recognized this possibility and pointed out that collisional deexcitation occurring in their high-pressure environment (≈ 0.1 atm) might cause a decrease in their measured luminous efficiency. We believe that the atmospheric tests demonstrate this to be true.

FST give an absolute luminous efficiency (the ratio of luminous energy to kinetic energy) in the photographic region of 0.006. From our experimental results, we would increase this to 0.025 for 20 km sec^{-1}. At this velocity, iron atoms possess about 100 ev with respect to the atmospheric molecules. Since iron radiation represents transition from levels about 2.5 ev above the ground state, the luminous efficiency of 0.025 results if each atom is

excited once. Quenching this radiation in three out of four excited atoms by deexciting collisions is required to explain the laboratory results. Cross sections for this process are unknown at these velocities. They are probably larger than the excitation cross section, but they almost certainly decrease with decreasing velocity. Since deexcitation occurs, of necessity, only after the atom has lost some velocity, the full effect of the larger deexcitation cross section will not be realized. The important factor in any quenching process is the number of collisions possible before spontaneous emission. The gas kinetic collision frequency at 0.1 atm, after the first few collisions have reduced the iron atoms to nearer thermal velocities, will be about 10^9 sec^{-1}. The corresponding number at our meteor altitudes is only 10^5 to 10^6 sec^{-1}. For the important iron lines — for example, multiplet No. 5 — the spontaneous emission probabilities are of the order to 2×10^7 sec^{-1} (Corliss and Tech, 1968). It is therefore plausible that collisional deexcitations could be important for the high-density experiments and negligible for the actual meteoric case.

Figure 21 shows a "best-guess" curve for τ_{pg} (Fe). We have combined results from all the data given therein to obtain this relationship. At high velocities we have accepted the FST velocity dependence but have increased their value of τ_{pg} by a factor of 4.5 to account for quenching. At low velocity we have imposed a steep velocity dependence that fits the observed iron data. We note that the nickel results, though weak, support this trend. It should be perfectly apparent from the probably errors in τ_{pg} (Table 3) that the best-guess curve is not uniquely determined. We present it as a first approximation that should be improved rather than used.

Retreating one more step from known facts, we have also proposed a τ_{pg} vs. V relationship for meteoric material of stony composition. We have assumed that

A. The iron abundance of the material is 15% by weight and iron is the only radiator in the photographic region at velocities below 20 km sec^{-1}. At these low velocities we take the luminous efficiency of stone as 15% that of iron.

B. As the velocity increases above this limit, other elements become increasingly important. This assumption is consistent with the general characteristics of bright-meteor spectra. For intermediate velocities ($20 < V < 30$), we propose a monotonic departure from the constant value of the corrected FST result.

C. The $n = 1$ velocity dependence on τ_{pg} derived from natural meteors is accurate for velocities above 30 km sec^{-1}. The relationship for intermediate velocities is faired to reach this dependence at 30 km sec^{-1}. A possible relationship embodying these factors is shown in Figure 22. As is the case for iron, the curve is intended for heuristic purposes only. Values for τ_{pg} for Harvard Meteors 19816 and 1242 are shown for comparison. These are derived from the published value of $\log \tau_0 = -18.91$ (Cook, Jacchia, and McCrosky, 1963), assuming equation (10) to be valid. The agreement with our curve is acceptable.

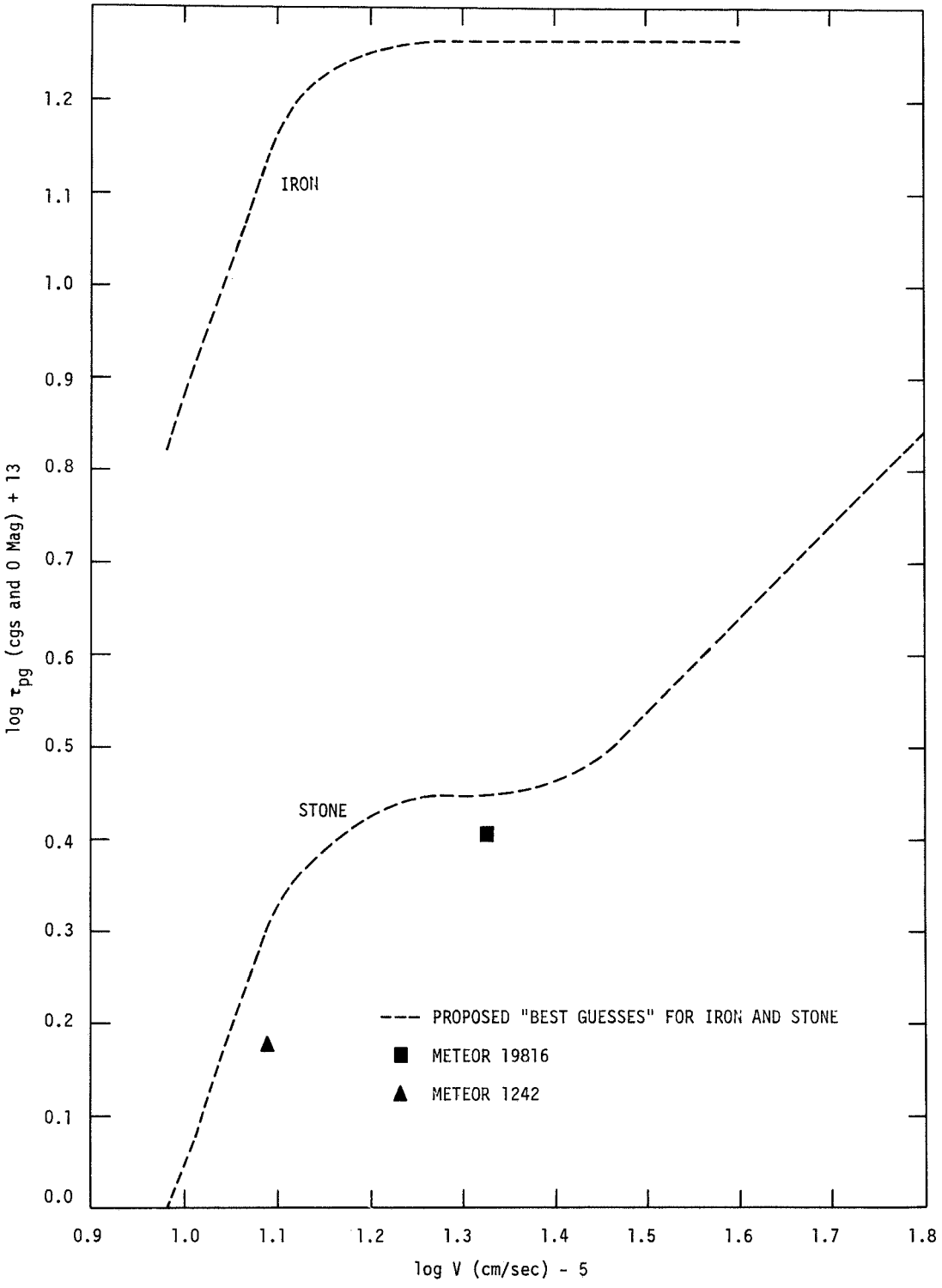

Figure 22. "Best-guess" luminosity efficiency of iron and meteoritic stone as a function of velocity.

6. REFERENCES

AYERS, W. G.

1968. Photographic photometry of artificial meteors. NASA Tech. Note D-4667, July, pp. 1-27.

COOK, A. F.

1955. On the constants of the physical theory of meteors (abstract). Astron. Journ., vol. 60, pp. 156-157.

COOK, A. F., JACCHIA, L. G., and McCROSKY, R. E.

1963. Luminous efficiency of iron and stone asteroid meteors. Smithsonian Contr. Astrophys., vol. 7, pp. 209-220.

CORLISS, C. H., and TECH, J. L.

1968. Oscillator strengths and transition probabilities for 3288 lines of Fe 1. National Bureau of Standards Monograph 108, March.

JACCHIA, L. G.

1949. Photographic meteor phenomena and theory. Harvard College Observatory and Center of Analysis, M.I.T., Tech. Rep. No. 3.

1957. On the "color index" of meteors. Astron. Journ., vol. 62, pp. 358-362.

FRIICHTENICHT, J. F., SLATTERY, J. C., and TAGLIAFERRI, E.

1968. A laboratory measurement of meteor luminous efficiency. Astrophys. Journ., vol. 151, pp. 747-758.

McCROSKY, R. E., and SOBERMAN, R. K.

1963. Results from an artificial iron meteoroid at 10 km/sec. Smithsonian Contr. Astrophys., vol. 7, pp. 199-208.

ÖPIK, E.

1933. Atomic collisions and radiation of meteors. Harvard Coll. Obs. Reprint Ser. I, no. 100, 39 pp.

1955. Meteor radiation, ionization and atomic luminous efficiency. Proc. Roy. Soc. London, ser. A, vol. 230, pp. 463-501.

VERNIANI, F.

1967. Meteor masses and luminosity. Smithsonian Contr. Astrophys., vol. 10, pp. 181-195.

WHIPPLE, F. L.

1949. The Harvard Photographic Meteor Program. Sky and Tel., vol. 8, pp. 90-93.

WHIPPLE, F. L., and HAWKINS, G. S.

1959. Meteors. In Handbuch der Physik, vol. 52, ed. by S. Flügge, Springer-Verlag Publ. Co., Berlin, pp. 519-564.

WHIPPLE, F. L., and JACCHIA, L. G.

1957. Reduction methods for photographic meteor trails. Smithsonian Contr. Astrophys., vol. 1, pp. 183-206.

APPENDIX

SUPER-SCHMIDT PHOTOMETRY OF ARTIFICIAL METEORS

APPENDIX

SUPER-SCHMIDT PHOTOMETRY OF ARTIFICIAL METEORS

The meteor light curves were obtained with the technique described by Whipple and Jacchia (1957). The apparent magnitudes of the meteor dashes (shutter openings) on the original films were estimated by visual comparison with out-of-focus trailed star images in the Harvard Standard Region C3 at $\alpha = 5^h$, $\delta = +15°$. The comparison films were taken on good nights at Wallops Island on x-ray and panchromatic emulsions identical with those used for the reentry observations. True magnitudes and colors of the C3 standard stars were photoelectrically determined at Harvard's Agassiz Station by one of us (CYS). The panchromatic magnitudes of these stars were obtained by a calibrated relation (McCrosky and Posen, 1968)

$$m_{pan} = V + 0.3(B - V) \quad , \tag{A-1}$$

where V is the yellow magnitude and B - V the color index in the U, B, V system; both quantities are available for most C3 stars from the Agassiz photometry.

To avoid systematic errors, the meteor dashes were always compared with star trails of similar length and degree of diffuseness. Because a meteor dash is often wider than a star trail of similar density, the effect of the relative trail widths was taken into account where necessary. The apparent meteor magnitudes were also corrected for the atmospheric extinction by the same method as was used by MS. The extinction correction was particularly important for the Trailblazer meteors that reentered at very low elevation angles. Hence, for meteors 1, 8, 9, and 10, the nightly extinction coefficient for each station was solved by use of 15 to 20 non-variable A-type stars on the calibration films taken for this purpose immediately after each reentry exposure. For the first three Nike-Cajun

launches, however, estimated coefficients, usually 0.3 to 0.4 mag per air mass in the blue region, were used in the reduction. Because the Nike-Cajun reentries never occurred at very large zenith distances from the stations (Table 3), the error due to an inexact extinction term could hardly exceed 0.2 mag. Meteor 10 was observed through four air masses and close to a region of obscuring clouds. Thus, the C3 stars as well as local stars in the immediate vicinity of the meteor were used in the photometry.

To reduce the apparent magnitudes to the absolute magnitudes at 100-km range, the usual corrections for the trailing velocity, the distance of the meteor from the film center, and the reciprocity failure of the emulsion have been made. The reciprocity correction to the panchromatic light curve of meteor 9 was +0.7 mag; no correction was applied to the photographic magnitudes. The shutter breaks (shutter closings) of several meteors were obliterated and the dashes blended together because of fragmentation of the meteoric body. Hence, a correction for this effect was required. The correction was estimated according to the last measured velocity and the reduced effect of shutter occultation on the meteor luminosity.

In general, all curves obtained from the two-station data exhibit reasonable agreement in magnitude scale and in shape. However, because the eye is not sensitive to small rapid-intensity variations, visual photometry tends to smooth out fine details. Finally, for each meteor we adopted a free-hand mean light curve that was used in the subsequent analysis of the luminous efficiency.

REFERENCE

McCROSKY, R. E., and POSEN, A.

1968. Special data-reduction procedures for Prairie Network meteor photographs. Smithsonian Astrophys. Obs. Spec. Rep. No. 273, pp. 1-88.

BIOGRAPHICAL NOTES

WENDELL G. AYERS received his B.S. degree in physics from Old Dominion University and his M.S. degree in optics from the University of Rochester. He is employed by the National Aeronautics and Space Administration, Langley Research Center. For a number of years, he was engaged in meteor research. He is currently working in advanced studies for Earth Orbital Experiment Programs.

RICHARD E. McCROSKY received his B.S. degree in physics from Harvard University in 1952 and his Ph.D. in astronomy from that university in 1956.

Dr. McCrosky holds joint appointments as Astronomer, Smithsonian Astrophysical Observatory, and Research Associate, Harvard University. He is also Scientist-in-Charge in the Smithsonian's optical meteor projects. His primary research specialties include photographic and spectral meteor studies.

CHENG-YUAN SHAO received the B.A. degree from the National Taiwan University in 1954 and the M.A. degree from Harvard University in 1962. He is an astronomer at Smithsonian Astrophysical Observatory and a senior research assistant at the Harvard College Observatory.

Mr. Shao has worked with Dr. R. E. McCrosky in the reduction and analysis of natural and artificial photographic meteors. He is also interested in stellar studies, especially of binaries, nonstable stars, and planetary nebulas.

NOTICE

This series of Special Reports was instituted under the supervision of Dr. F. L. Whipple, Director of the Astrophysical Observatory of the Smithsonian Institution, shortly after the launching of the first artificial earth satellite on October 4, 1957. Contributions come from the Staff of the Observatory.

First issued to ensure the immediate dissemination of data for satellite tracking, the reports have continued to provide a rapid distribution of catalogs of satellite observations, orbital information, and preliminary results of data analyses prior to formal publication in the appropriate journals. The Reports are also used extensively for the rapid publication of preliminary or special results in other fields of astrophysics.

The Reports are regularly distributed to all institutions participating in the U. S. space research program and to individual scientists who request them from the Publications Division, Distribution Section, Smithsonian Astrophysical Observatory, Cambridge, Massachusetts 02138.